Title

Interaction Landscape of K29-Linked Ubiquitin Signaling Revealed by a Linkage-Specific Synthetic Antigen-Binding Fragment

Authors

Yuanyuan Yu[1,†], Qingyun Zheng[2,†], Satchal K. Erramilli[1,†], Man Pan[1,†,*], Seongjin Park[1], Yuan Xie[1], Jingxian Li[1], Jingyi Fei[1], Anthony A. Kossiakoff[1,*], Lei Liu[2,*], Minglei Zhao[1,*]

Affiliations

[1]Department of Biochemistry and Molecular Biology, The University of Chicago, Chicago, IL, 60637, USA.

[2]Department of Chemistry, Tsinghua University, Beijing, 100084, China.

[†]These authors contributed equally.

Contact Info

[*]Corresponding authors:

Minglei Zhao: mlzhao@uchicago.edu

Lei Liu: lliu@mail.tsinghua.edu.cn

Anthony Kossiakoff: koss@bsd.uchicago.edu

Man Pan: panm@uchicago.edu

Summary

Protein ubiquitination shows remarkable topological and functional diversity through the polymerization of ubiquitin via different linkages. Deciphering the cellular ubiquitin code is of central importance to understand the physiology of the cell. Among the eight possible linkages, K29-linked polyubiquitin is a relatively abundant type of polyubiquitin in both human and yeast cells (Tsuchiya et al., 2018). However, the lack of specific binders as tools to detect K29-linked polyubiquitin has prevented further understanding of its function. In this study, we screened and characterized a synthetic antigen-binding fragment that can specifically recognize K29-linked polyubiquitin. We determined the crystal structure of this fragment bound to K29-linked diubiquitin, which revealed the molecular basis of sAB-K29 specificity. We identified the involvement of K29-linked ubiquitination in RNA processing, the proteotoxic stress response and cell cycle regulation. In particular, we showed that K29-linked ubiquitination is enriched in the midbody and downregulation of the K29-linked ubiquitination signal arrests cells in G1 phase.

Keywords

K29-linked polyubiquitination; sAB-K29; cell cycle; proteotoxic stress; midbody

INTRODUCTION

Protein ubiquitination is a dynamic posttranslational modification involved in nearly all aspects of eukaryotic cells (Komander and Rape, 2012; Swatek and Komander, 2016; Yau and Rape, 2016). Ubiquitin, a 76-amino acid protein, can be covalently attached to its substrate through an isopeptide bond between its C-terminal carboxyl group and the side-chain amino group of a lysine residue on the substrate, initiating the process of ubiquitination. The substrate protein can be modified by either a single ubiquitin, called monoubiquitination, or a chain of ubiquitin molecules, termed polyubiquitination. To form a ubiquitin chain, the second and subsequent ubiquitin molecules need to be conjugated to one of the seven lysine residues in ubiquitin (K6, K11, K27, K29, K33, K48, and K63) or the N-terminal amino group of the first methionine residue (M1) on the preceding ubiquitin molecule (Figure 1A). Hence, a total of eight linkages between any of two covalently linked ubiquitin molecules exist in vivo, which makes polyubiquitination an extremely diverse posttranslational modification (Komander and Rape, 2012). Recently, branched and heterotypic ubiquitin chains were also discovered in eukaryotic cells, further expanding the complexity of ubiquitination (Haakonsen and Rape, 2019; Lopez-Mosqueda and Dikic, 2014; Meyer and Rape, 2014). Ubiquitin chains with different linkages have different topologies and structures, creating a multitude of distinct signals, which results in distinct cellular outcomes. For instance, K48-linked polyubiquitin chains adopt a closed conformation and target their substrate proteins to the proteasome for degradation (de la Pena et al., 2018; Ding et al., 2019; Dong et al., 2019). In contrast, K63-linked polyubiquitin chains adopt an open conformation and regulate proteasome-independent signaling pathways such as DNA repair, inflammatory signaling, and endocytosis (Wang et al., 2012). Other types of polyubiquitin chains have also been reported to adopt distinct structures and perform specific cellular roles (Ikeda and Dikic, 2008; Kulathu and Komander, 2012; van Huizen and Kikkert, 2019). Together, these ubiquitination signals are referred to as the 'ubiquitin code'.

The cellular ubiquitin code is dynamic and tightly regulated by a cascade of enzymatic events that involve three different enzymes: a ubiquitin-activating enzyme (E1), a ubiquitin-conjugating enzyme (E2) and a ubiquitin ligase (E3) (Scheffner et al., 1995). Ubiquitination is initiated by the activation of ubiquitin by E1, followed by its conjugation to an E2, after which it is ligated to the lysine residues of target proteins or a preceding ubiquitin molecule by an E3 ligase. Ubiquitination can be reversed by an opposing process termed deubiquitination, catalyzed by deubiquitinating enzymes (DUBs) (Mevissen and Komander, 2017). DUBs can cleave the isopeptide bonds between ubiquitin and its substrates or within ubiquitin chains and thus reverse the ubiquitination process. The ubiquitin code is translated to distinct cellular processes by interactions with ubiquitin-binding domains (UBDs) in many cellular proteins (Dikic et al., 2009; Hicke et al., 2005). These UBDs are diverse domains that can distinguish between different ubiquitin chain linkages. In human cells, more than 100 kinds of UBDs exist in numerous cellular proteins. Together, the specific E1-E2-E3 system, DUBs, and UBDs constitute the writers, erasers, and readers, respectively, of a specific ubiquitin code.

Linkage-specific binders play a key role in decoding the ubiquitin code with various topologies. Newton et al. developed two linkage-specific antibodies that specifically recognize K48- and K63-linked polyubiquitin chains and used them to reveal that polyubiquitin editing is a general mechanism to attenuate innate immune signaling (Newton et al., 2008). Matsumoto et al. engineered a K11-linked polyubiquitin linkage-specific antibody and used it to demonstrate that K11-linked chains are critical regulators of the degradation of mitotic proteins (Matsumoto et al., 2010). Matsumoto et al. further engineered a linear polyubiquitin (M1-linked) linkage-specific antibody (Matsumoto et al., 2012), which was an essential tool used to uncover the role of linear chains in immune responses (Keusekotten et al., 2013). Martin et al. characterized linkage-specific "affimer" reagents that recognize K6- and K33-linked polyubiquitin chains and used the K6 affimer to show that HUWE1 is the main E3 ligase for the K6-linked polyubiquitin chain, which modifies mitofusin-2 (Michel et al., 2017). For a heterotypic polyubiquitin chain, Richard et

al. engineered a bispecific antibody that recognizes K11/K48-linked chains and used it to show that mitotic regulators, misfolded nascent polypeptides, and pathological Huntingtin variants are endogenous substrates of K11/K48-linked polyubiquitin chains (Yau et al., 2017). To date, with the exception of the K29-linked polyubiquitin chain, all other homotypic ubiquitin chains have been reported via linkage-specific detection tools (Michel et al., 2017). Notably, K29-linked ubiquitin chains are one of the most abundant linkage types, according to recent studies in which the amounts of different linkages in eukaryotic cells were quantified (Tsuchiya et al., 2018), and follow only K48- and K63-linked polyubiquitin chains in terms of abundance. Moreover, K29-linked ubiquitin chains were recently reported to play a nonproteolytic role in pathogen regulation by modifying the PB2 replication factor (Karim et al., 2020). Therefore, the development of a specific detection tool to reveal pathways that depend on K29-linked chains awaits.

In this study, we developed and characterized a synthetic antigen-binding fragment (sAB) that can specifically recognize K29-linked ubiquitin chains at nanomolar concentrations by screening a phage display library. We determined the crystal structure of the sAB in complex with K29-linked diubiquitin (diUb) and elucidated the specific interactions between the two components around the isopeptide bond. Through a series of experiments, including pull-down assays, mass spectrometry and immunofluorescent imaging, we demonstrated that sAB-K29 is a high-quality tool for functional studies. Moreover, K29-linked ubiquitination was identified to be widely involved in protein homeostasis, RNA processing, the stress response, and especially cell cycle regulation in HeLa cells. Interestingly, we found that K29-linked ubiquitination was particularly enriched in the midbody at the telophase of mitosis, which was not observed in other stages of the cell cycle. The knockdown of K29-linked ubiquitination by a specific DUB led to arrest of the cell cycle at G1/S phase. In summary, we have established that K29-linked ubiquitin chains are important carriers in different cellular signaling pathways.

RESULTS

Selection of K29-linked polyubiquitin-specific sAB (sAB-K29) from a phage display library

sABs have been successfully developed as linkage-specific binders for M1-, K11-, K48-, and K63-linked ubiquitin, as mentioned above. They are functionally and structurally similar to antigen-binding fragments (Fabs) and can be selected from a synthetic phage display library (Miersch et al., 2015). To obtain a K29-linked ubiquitin-specific binder, we first chemically synthesized biotinylated K29-linked diUb following previously developed methods (Pan et al., 2016). A polyethylene glycol (PEG) linker was introduced between the diUb and biotin moieties. The synthetic route is briefly summarized in Figure S1A. We conducted reverse-phase high-performance liquid chromatography (RP-HPLC) followed by liquid chromatography-mass spectrometry (LC-MS) to verify the mass of the product (Figure S1B). Next, we refolded the product using a standard dialysis method and collected the circular dichroism (CD) spectrum of the final product (Figure S1C). The CD spectrum of the synthesized K29-linked diUb showed an ellipticity near identical to that of the ubiquitin monomer (monoUb), suggesting correct folding of the diUb (Pan et al., 2019).

We subsequently generated a K29-linked diUb-specific sAB from a phage display library, known as Library E, based on a humanized antibody Fab scaffold (Miller et al., 2012). This in vitro technique allows for exquisite control over sAB selection conditions (Paduch et al., 2013). We took advantage of this methodology by using an excess of monoUb in solution (Figure 1B) to generate a linkage-specific binder, which we termed sAB-K29 and characterized further as described below.

Structural characterization of sAB-K29 in complex with K29-linked diUb

To enable crystal screening of K29-linked diUb at a high concentration, a large quantity of K29-linked diUb was enzymatically prepared using a previously published method (Kristariyanto et

al., 2015b). Ubiquitin was mixed with UBA1, UBE2L3, and UBE3C for polyubiquitin chain formation. The resulting polyubiquitin was a mixture of mainly K48- and K29-linked chains. vOTU, a DUB that does not cleave K29-linked chains, was introduced to the mixture to remove the K48-linked chains. Finally, K29-linked diUb was separated from monoUb and polyubiquitin using anion exchange chromatography (Figure S2A). To obtain the complex of sAB-K29 and K29-linked diUb, we mixed purified K29-linked diUb with sAB-K29 at a molar ratio of 1.5:1 and ran the mixture through gel filtration (Figure S2B and C). The stable complex was subjected to crystallization screening (see methods for details). Diffraction-quality crystals appeared from a reservoir solution containing 0.1 M phosphate-citrate and 40% v/v PEG 300 (Figure S2D). Diffraction data to 2.9 Å resolution were collected at the Advanced Photon Source at Argonne National Lab (Supplemental Table S1).

The complex structure shows a 1:1 stoichiometry of sAB-K29 and K29-linked diUb (Figure 1C). There are three binding interfaces between the complementarity-determining regions (CDRs) of sAB-K29 and diUb, as shown in Figure 1C. The left interface (black box) involves the heavy chain of sAB-K29 (CDR-H1 and H2) and the distal ubiquitin molecule. The right interface (gray box) involves the light chain of sAB-K29 (CDR-L1 and L3) and the proximal ubiquitin molecule. The middle interface (red box) involves both chains (CDR-H2, H3 and L3) and the linker between the two ubiquitin molecules. Hydrogen bonding networks and van der Waals interactions mainly contributed by tyrosine and serine residues dominate the interfaces (Figure 2D). Each of the three interfaces recognizes an essential piece of the diUb, namely, the proximal ubiquitin, distal ubiquitin, and linker. Together, they form the basis for specific recognition. Notably, the patch containing I44 on both ubiquitin molecules is not involved in the binding interface. Only the patch containing I36 of the distal ubiquitin molecule is involved in the interaction with the heavy chain of sAB-K29 (Figure S2E). Compared to the crystal structure of K29-linked diUb (PDB accession code: 4S22), the diUb in this complex adopts a more compact

conformation, with the proximal ubiquitin molecule rotated approximately 60 degrees compared to that in the other structure (Figure S2F).

In vitro characterization of sAB-K29

We first performed single-point competitive phage enzyme-linked immunosorbent assay (ELISA) using M13 phage-displayed sAB-K29. The signal decreased when K29-linked diUb, but not K27- or K33-linked diUb, was used as the competitor in solution, suggesting its specificity towards K29-linked diUb (Figure S3A). Next, we tested the specificity of sAB-K29 against diUb of all linkage types (100 ng) by Western blotting. sAB-K29 recognized only K29-linked diUb and showed no cross-reactivity with other linkage types even after long exposure (Figure 2A). We further performed Western blotting against serially diluted K29-linked diUb from 25 ng to 0.78 ng. The results suggested that sAB-K29 is at least 320-fold more sensitive for K29-linked diUb than the other diUbs tested (Figure 2B). Interestingly, a single point mutation in the heavy chain (CDR-H3) of sAB-K29, Y112 (red box, Figure 1D), completely abolished the recognition of K29-linked diUb by sAB-K29, as shown by Western blotting. We measured the binding affinity of sAB-K29 and K29-linked diUb using surface plasmon resonance (SPR) and ELISA. By SPR, the dissociation constant (K_D) was measured to be 0.915 nM, which was in agreement with the EC50 of 1.46 nM measured by ELISA.

Next, we tested whether sAB-K29 can be used to detect K29-linked polyubiquitin chains. We mixed ubiquitin with UBA1, UBE2L3, and UBE3C and monitored assembly of the polyubiquitin chain using Western blotting. UBE3C is known to produce a mixture of mainly K48- and K29-linked polyubiquitin chains (Michel et al., 2015). K29C mutant ubiquitin, which cannot form K29-linked polyubiquitin chains, was included as a control. The results of Western blotting showed that sAB-K29 specifically recognized K29-linked polyubiquitin chains (Figure 2F, left), although the K29C mutant did not prevent the assembly of K48-linked polyubiquitin chains, as detected with a commercial anti-ubiquitin antibody (Figure 2F, right). The Y112A sAB-K29

mutant could not recognize the K29-linked polyubiquitin chain, as shown by Western blotting (Figure S3B). We further assembled K11-, K48- and K63-linked polyubiquitin chains using UBE2S, E2-25K, and Ubc13/Mms2, respectively, and monitored the reactions using Western blotting. Again, sAB-K29 could detect only the K29-linked polyubiquitin chains produced by the UBE3C system, not polyubiquitin chains with other types of linkages (Figure 2G). Together, these results suggest that sAB-K29 can be used as a tool to specifically detect K29-linked polyubiquitin chains in vitro.

K29-linked ubiquitination is involved in protein homeostasis, RNA processing, the stress response, and cell cycle regulation

To further investigate the function of K29-linked ubiquitination in cells, we introduced a biotin tag at the C-terminus of the heavy chain of sAB-K29 using sortase-catalyzed ligation (Antos et al., 2016; Li et al., 2014). A polyethylene glycol (PEG) linker between the biotin moiety and sAB-K29 was introduced to increase the flexibility. Using biotinylated sAB-K29, we first performed pull-down experiments against monoUb and diUb of all linkage types. The results showed that K29-linked diUb was specifically pulled down (Figure 3A). Next, we tested whether the pull-down assay would work in a crowded environment by mixing HeLa cell lysate with K29-linked diUb, K48-linked diUb, and monoUb and performed Western blotting using an anti-ubiquitin antibody. Only K29-linked diUb was pulled down with high-molecular-weight endogenous species (Figure 3B), suggesting that biotinylated sAB-K29 can be used as a specific tool for cellular pull-down assays.

To elucidate the function of K29-linked ubiquitination, we conjugated biotinylated sAB-K29 to magnetic streptavidin beads and used the beads to capture K29-linked ubiquitinated proteins from HeLa cell lysates. The enriched proteins were eluted with 8 M urea and subjected to tandem mass tag (TMT) labeling mass spectrometry analysis. Unconjugated streptavidin beads were used in a control experiment (Figure S3C and D). Significant hits from the mass

spectrometry results ($p < 0.05$) were converted to gene IDs and subjected to gene ontology (GO) analysis. GO enrichment analysis for cellular components showed that K29-linked ubiquitination is present in the spliceosome, proteasome, nuclear pore, stress granules, and in particular several important complexes involved in mitosis, including the centrosome, kinetochore, mitotic spindle, and midbody (Figure 3C). GO enrichment analysis for biological processes indicated that the hits were enriched in RNA processing, transcriptional regulation, protein homeostasis, the stress response, and cell cycle regulation (Figures 3D-F, Figure S3F, see supplemental materials for details). The last three categories were further investigated in this work. Specifically, among hits enriched in the protein homeostasis category, VCP (also known as p97 or Cdc48, an AAA+ protein involved in the processing of ubiquitinated proteins) and its diverse cofactors, three major autophagic adapters, and many proteasome subunits were identified (Figures 3D). Among hits enriched in the stress response category, stress granule components and some heat shock and oxidative stress responsive proteins were identified (Figures 3E). Among hits enriched in the cell cycle category, proteins that control different stages of the cell cycle, including those involved in DNA replication, spindle assembly, chromatin condensation and midbody formation, were identified (Figures 3F).

Proteotoxic stress induced K29-linked ubiquitination

To further investigate the results of mass spectrometry and GO analysis, we costained HeLa cells for K29-linked ubiquitin with VCP, the 20S proteasome (the core machinery involved in cellular protein degradation), and eukaryotic translation initiation factor 3 subunit B (EIF3B, enriched in stress granules) using sAB-K29 and the corresponding antibodies. The results showed that K29-linked polyubiquitin was widely distributed in the cytoplasm and nucleus and generally colocalized with VCP and the 20S proteasome (Figures 4A, S4A and S4B), as well as EIF3B in the cytoplasm (Figure 4A). In addition, K29-linked polyubiquitin formed bright puncta in the cytoplasm of some cells (arrowheads, Figure 4A). It was also found in some large

cytoplasmic droplets and costained with VCP and the 20S proteasome, but not EIF3B or K48-linked polyubiquitin (arrows, Figures 4A and S4C).

To further explore this phenomenon, we treated HeLa cells with CuET (bis-(diethyldithiocarbamate)-copper), a drug that targets NPLOC4 (Pan et al., 2020; Skrott et al., 2017) (also known as Npl4, the most common adapter of VCP); MG132, a proteasome inhibitor; and sodium arsenite, which triggers the stress response. All three compounds dramatically increased the level of K29-linked polyubiquitination in the cell lysate, as shown by Western blot analysis (Figure 4B). The cellular VCP level did not change much upon treatment with CuET or MG132 (Figure S4D). Interestingly, CuET did not induce a dramatic increase in the total ubiquitin level, unlike MG132 (Figure S4D), which indicated that K29-linked ubiquitination might be closely associated with the VCP/NPLOC4 complex. We also performed immunofluorescent staining experiments after the treatments. Many more K29-linked polyubiquitin puncta were observed after CuET treatment, and these puncta colocalized with VCP (Figure 4C). Stress granules that stained positive with sAB-K29 were observed after treatment with MG132 or sodium arsenite, which colocalized with the 20S proteasome or EIF3B, respectively (Figure 4C). Furthermore, the staining was specific, as no signal was observed when a control sAB was used (Figure S4E).

To further confirm the involvement of K29-linked polyubiquitination in the stress response, we treated HeLa cells with heat shock by exposure to 45 °C, which can also lead to stress granule formation, as previously described (Jolly et al., 1999). We found that K29-linked polyubiquitin colocalized with both EIF3B and G3BP1 in the resulting stress granules (Figure 4D). G3BP1, another biomarker of cytosolic stress granules (Tsai et al., 2016), was identified as a hit from our mass spectrometry results (Figure 3E). Interestingly, we found that stress granules from sodium arsenite treatment were VCP positive, whereas heat shock for 30 minutes resulted in VCP-negative stress granules (Figure S4F). Together, our experiments suggest that

K29-linked ubiquitination is upregulated in the proteotoxic stress response and enriched in the granular structures formed after exposure to stress.

Reduction in the level of K29-linked ubiquitination led to cell cycle arrest

As shown by the results of mass spectrometry and GO analysis, many cell cycle-related proteins and complexes were detected (Figure 3C and F). To further investigate this phenomenon, we designed a method to reduce the level of K29-linked ubiquitination in cultured cells. A reduction in K29-linked ubiquitination was achieved by transfecting the cells with a truncated human DUB, TRABID (residue range 245-697, noted as Tra hereafter). According to previous studies, the Tra construct preferentially targets K29-linked ubiquitin chains, although it shows minimal activity against K63-linked ubiquitin chains (Licchesi et al., 2011). As expected, HeLa cells transfected with the Tra construct showed significantly decreased levels of K29-linked polyubiquitinated proteins, as detected by sAB-K29 (Figure 5B and C). We also tested the level of K63-linked polyubiquitinated proteins using a commercially available antibody. There was no significant difference in K63-linked polyubiquitination between Tra and vector transfection (Figure S5A).

Next, we performed cell cycle analysis of HeLa cells transfected with either the Tra construct or the empty vector using flow cytometry. Among HeLa cells transfected with the Tra construct, 14% of the cells showed a reduced level of K29-linked ubiquitination, as detected by sAB-K29, whereas only 1.7% of the cells transfected with the empty vector were found in the same region (Q1, Figure 5D). The reduced level of K29-linked ubiquitination in the Q1 cells was due to expression of the Tra construct as shown by the signal of cMyc channel (Figure S6A). Cell cycle analysis of Q1 cells transfected with the Tra construct showed that 93.0% of the cells were in G1 phase, 10.8% of cells were in S phase, and almost no cells were in G2 phase, which was significantly different from the cell cycle distribution of Q2 cells transfected with the empty vector (Figure 5D and E) and normal HeLa cells (Figure S6B). We also tested A549 cells with the

same experimental setup and observed similar results (Figure S6C and D). Together, these results suggest that K29-linked ubiquitination is essential for cell cycle progression. A reduction in the level of K29-linked ubiquitination arrested the cells in G1 phase.

K29-linked ubiquitination is involved in midbody assembly

To further investigate the relevance of K29-linked ubiquitination to cell cycle regulation, we performed immunofluorescent staining of HeLa cells at different stages of the cell cycle using sAB-K29 (Figure 6A). As shown by the results of Western blotting, K29-linked ubiquitination occurred in all stages of mitosis, but the level of K29-linked ubiquitination was slightly reduced in cells during mitosis compared to asynchronized cells (Figure S7A). Unexpectedly, the K29-linked ubiquitination signal was especially enriched around the midbody in telophase. Based on localization of the K29-linked polyubiquitin signal and the morphology of the daughter cells, we further divided telophase into four stages termed telophase 1-4 (Figure 6B). At telophase 1, the K29-linked polyubiquitin signal formed a bright dot in the middle of two daughter cells. A dark zone appeared at telophase 2. The daughter cells and K29-linked polyubiquitin signal were further apart in telophase 3. Finally, the K29-linked polyubiquitin signal formed a dim ring in the midbody at telophase 4, which was visualized by three-dimensional stochastic optical reconstruction microscopy (3D STORM, Figure S7B, Movies S1A and S1B). The positional and morphological changes in the K29-linked polyubiquitin signal during telophase suggest that the modification was dynamic and tightly regulated. We also performed immunofluorescent staining following a pre-extraction protocol to remove weakly bound proteins and found that the K29-linked polyubiquitin signal was still specifically enriched around the midbody at telophase, indicating that K29-linked ubiquitination occurs on strongly interacting or covalently modified midbody components (Figure S7C and D).

To test whether K29-linked ubiquitination at the midbody is a degradation signal, we performed immunofluorescent costaining using sAB-K29. K29-linked polyubiquitin colocalized

with neither the 20S proteasome (Figure 6C) nor K48-linked polyubiquitin (Figure 6D) around the midbody at telophase, indicating that K29-linked ubiquitination around the midbody does not function as a degradation signal. Previously, VCP was reported to participate in midbody assembly (Ramadan et al., 2007); therefore, we tested the colocalization of VCP with K29-linked polyubiquitin by costaining and observed their colocalization at telophase 1 and 2 but not late telophase 4 (Figure 6E). Therefore, K29-linked ubiquitination may be a specific signal for VCP-mediated midbody assembly, but this hypothesis requires further investigation.

Identification of midbody proteins modified with K29-linked polyubiquitin

To identify the substrates of K29-linked ubiquitination in the midbody, we sought to perform immunoprecipitation (IP) under denaturing conditions to minimize the presence of noncovalently bound proteins. We first tested the specificity of sAB-K29 under various denaturing conditions and found that biotinylated sAB-K29 could specifically pull down K29-linked diUb in 1 M urea (Figures 7A and S3E). Next, we synchronized HeLa cells to telophase to maximize the abundance of the midbody and lysed the cells using 8 M urea. The lysate was further diluted in 1 M urea, followed by IP using biotinylated sAB-K29. The enriched proteins were separated on an SDS-PAGE gel and subjected to label-free quantitative mass spectrometry analysis.

Several midbody proteins, such as TBK1, PLK1, INCENP, and MKLP1, were enriched with respect to the control (Figure 7B). Through immunofluorescent costaining, we observed that TBK1, PLK1 and INCENP colocalized with the K29-linked polyubiquitin signal (top row, Figure 7C). Interestingly, MKLP1 did not colocalize with the K29-linked polyubiquitin signal at telophase 2, but with the progression of cytokinesis, it gradually colocalized with the ring structure consisting of K29-linked polyubiquitin formed at telophase 4 (bottom row, Figure 7C). We also performed immunofluorescent staining for a well-known midbody regulator, Aurora B, which did not show up as a hit in our mass spectrometry analysis. As expected, the K29-linked polyubiquitin signal colocalized with Aurora B in the midbody (Figure S6D), suggesting that sAB-

K29 pulled down only K29-linked ubiquitinated substrates under denaturing conditions. We further validated these results by IP and Western blotting. We used antibodies against TBK1, PLK1, INCENP and MLKP1 to pull down proteins in the lysate of HeLa cells synchronized to telophase and used sAB-K29 to detect K29-linked ubiquitination (Figure 7D). Alternatively, we used sAB-K29 to pull down proteins in the cell lysate and used antibodies against the respective proteins for Western blotting (Figure 7E). As expected, in both experiments, polyubiquitinated substrates with a high molecular weight were observed. In summary, we identified TBK1, PLK1, INCENP and MLKP1 as potential substrates of K29-linked ubiquitination during midbody assembly. The detailed roles of their modification require further investigation.

DISCUSSION

K29-linked ubiquitination is one of the most abundant polyubiquitin linkage type following K48-linked ubiquitination which serves as a signal for proteasome-mediated degradation. The cellular function of K29-linked ubiquitination is not clear because it is the only linkage type that does not have a specific binder as a tool for detection (Michel et al., 2017). In this study, we filled in this gap by developing and characterizing a linkage-specific sAB against K29-linked polyubiquitin, named sAB-K29, using synthetic K29-linked diUb. We determined the crystal structure of sAB-K29 in complex with recombinant K29-linked diUb and elucidated its binding specificity at the atomic level. Using sAB-K29 as a tool, we discovered that K29-linked ubiquitination is mainly involved in RNA processing, the stress response, and cell cycle regulation. A reduction in K29-linked polyubiquitin by transfection of a K29-linkage-specific DUB construct resulted in cell cycle arrest. Furthermore, we found that the K29-linked polyubiquitin signal was specifically enriched around the midbody during telophase of mitosis and identified potential substrates of this type of modification.

We explored the role of K29-linked ubiquitination in the stress response and found that K29-linked ubiquitin was enriched in puncta, liquid droplets, and stress granules in the cytosol upon proteotoxic stress. The function of this modification may not be linked to protein degradation; instead, it may serve as a localization signal since K29-linked ubiquitin did not always colocalize with the 20S proteasome and K48-linked ubiquitin (Figure 6C and D). Moreover, we treated HeLa cells with puromycin, an antibiotic drug that can be incorporated into nascent chains during translation, and found that HeLa cells with a reduced level of K29-linked ubiquitination did not show obvious accumulation of nascent chains (Figure S5F and G), which suggests a nondegradative role for K29-linked ubiquitination.

We also explored the role of K29-linked ubiquitination in cell cycle regulation. A reduction in K29-linked ubiquitination did not affect the cellular levels of some key regulators, including cyclin A, CDC27, STAT3, and cyclin D1 (Figure S5B-E), which also pointed to a nondegradative role for this modification. The fact that K29-linked ubiquitin did not colocalize with K48-linked ubiquitin during costaining and formed high-molecular-weight species during Western blotting suggests that K29-linked ubiquitin chains may be homotypic. From the mass spectrometry results, several cullin family E3 ligases, including CUL1, CUL3, CUL4A, and CUL4B, were suggested to serve as the “writer” of this modification (Figure 7B). Further experiments to identify the entire E3 complex responsible for this modification are necessary.

K29-linked ubiquitination was specifically enriched around the midbody during telophase of mitosis. This modification was dynamic, as the localization and structure changed over the progression of mitosis (Figure 6A). We identified multiple midbody proteins that could be substrates of K29-linked ubiquitination from IP experiments under denaturing conditions. The fact that VCP, but not the proteasome, colocalized with the K29-linked polyubiquitin signal again suggests a nondegradative role for this modification. VCP is an ATPase involved in processing various ubiquitinated cellular proteins (Meyer et al., 2012). Our results suggest that VCP is widely associated with K29-linked ubiquitination under normal conditions, during stress, or during cell division. Therefore, it may serve as a key processor for this modification. However, the exact role of K29-linked ubiquitination in midbody assembly requires further investigation.

Acknowledgements

Funding for this work was, in part, provided by the Catalyst Award from the Chicago Biomedical Consortium. This work was supported by Chicago Biomedical Consortium Catalyst Award C-086 to M.Z. We thank the National Key R&D Program of China (No. 2017YFA0505200), NSFC (91753205) for financial support.

Author Contributions

Y.Y., M.P., L.L. and M.Z. designed all the experiments and interpreted the results. S.K.E and A.A.K performed the sAB selection and evaluation; Y.Y., Q.Z., and M.P. synthesized all diubiquitin molecules and carried out the related biochemical characterizations. Y.Y., J.L. and M.Z. performed crystal screening and data processing. Q.Z., Y.Y. and M.P. performed and interpreted the LC-MS/MS experiments. Y.Y., Y.X., S.P., and J.F. performed the cell-based imaging experiments. M.Z., M.P., and Y.Y. wrote the paper. M.Z., L.L. and A.A.K supervised the project.

Declaration of Interests

The authors declare no competing interests.

FIGURE LEGENDS

FIGURE 1

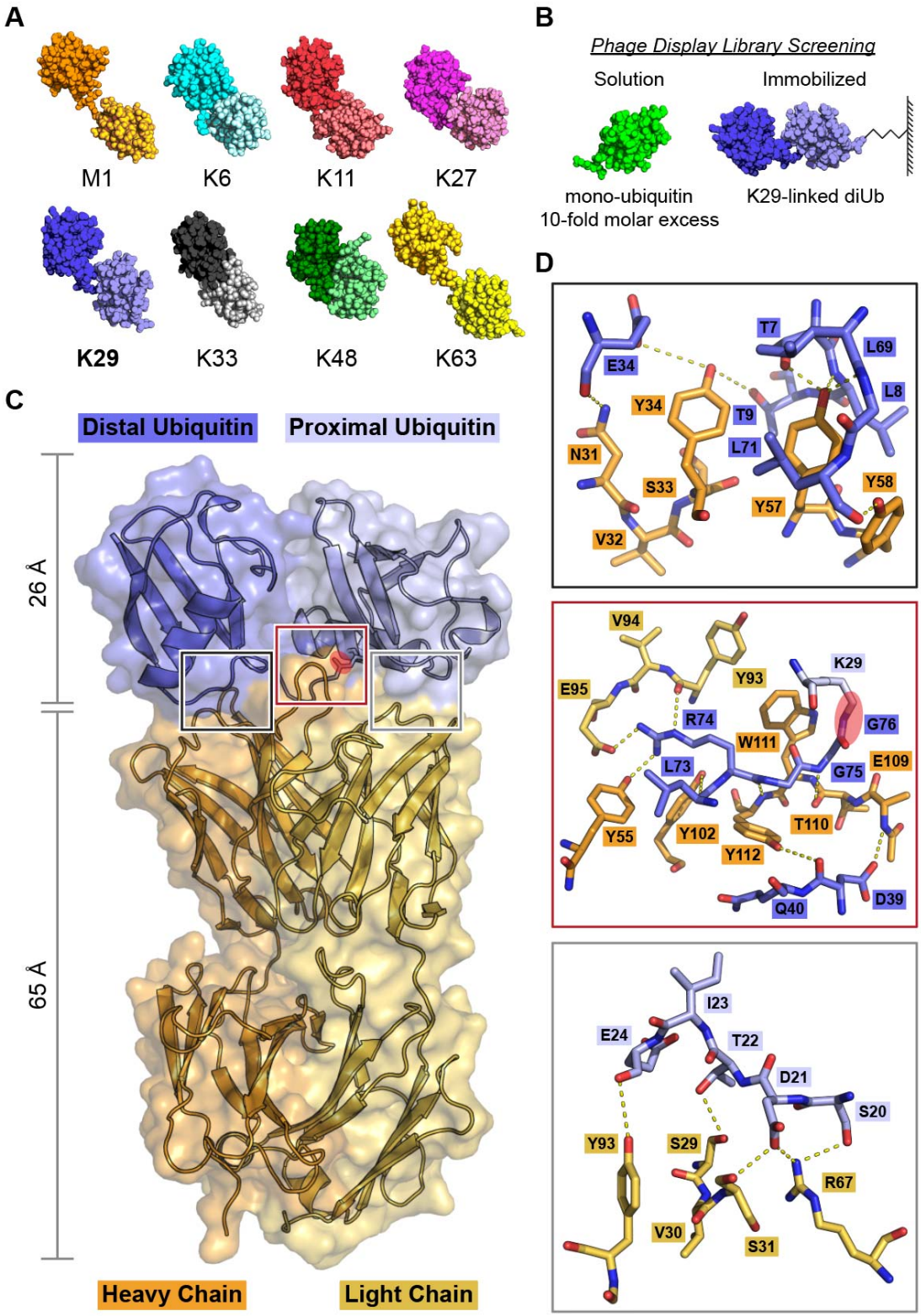

Figure 1. Screening for a K29-linked ubiquitin chain-specific binder and the complex structure of sAB-K29 and K29-linked diubiquitin

(A) Crystal structures of diubiquitin molecules with eight possible linkages. The K29-linked ubiquitin chain was the focus of this study.

(B) Screening of a phage display library of engineered Fabs using immobilized synthetic K29-linked diubiquitin. Monoubiquitin at a 10-fold molar excess was used for negative selection.

(C) Crystal structure of sAB-K29 in complex with K29-linked diubiquitin determined at a 2.9 Å resolution (Supplemental Table S1). Color code: dark orange, heavy chain of sAB-K29; light orange, light chain of sAB-K29; dark blue, distal ubiquitin; light blue, proximal ubiquitin. The isopeptide bond between the C-terminus of the distal ubiquitin molecule and K29 of the proximal ubiquitin molecule is highlighted with a red oval.

(D) Zoomed-in views of the three binding interfaces between sAB-K29 and diubiquitin. Top, binding interface between the heavy chain of sAB-K29 and the distal ubiquitin molecule; middle, binding interface between both the heavy and light chains of sAB-K29 and the linker region of the diubiquitin molecule; bottom, binding interface between the light chain of sAB-K29 and the proximal ubiquitin molecule. Potential hydrogen bonds are shown as dotted lines. The isopeptide bond in the middle panel is highlighted with a red oval.

449 **FIGURE 2**

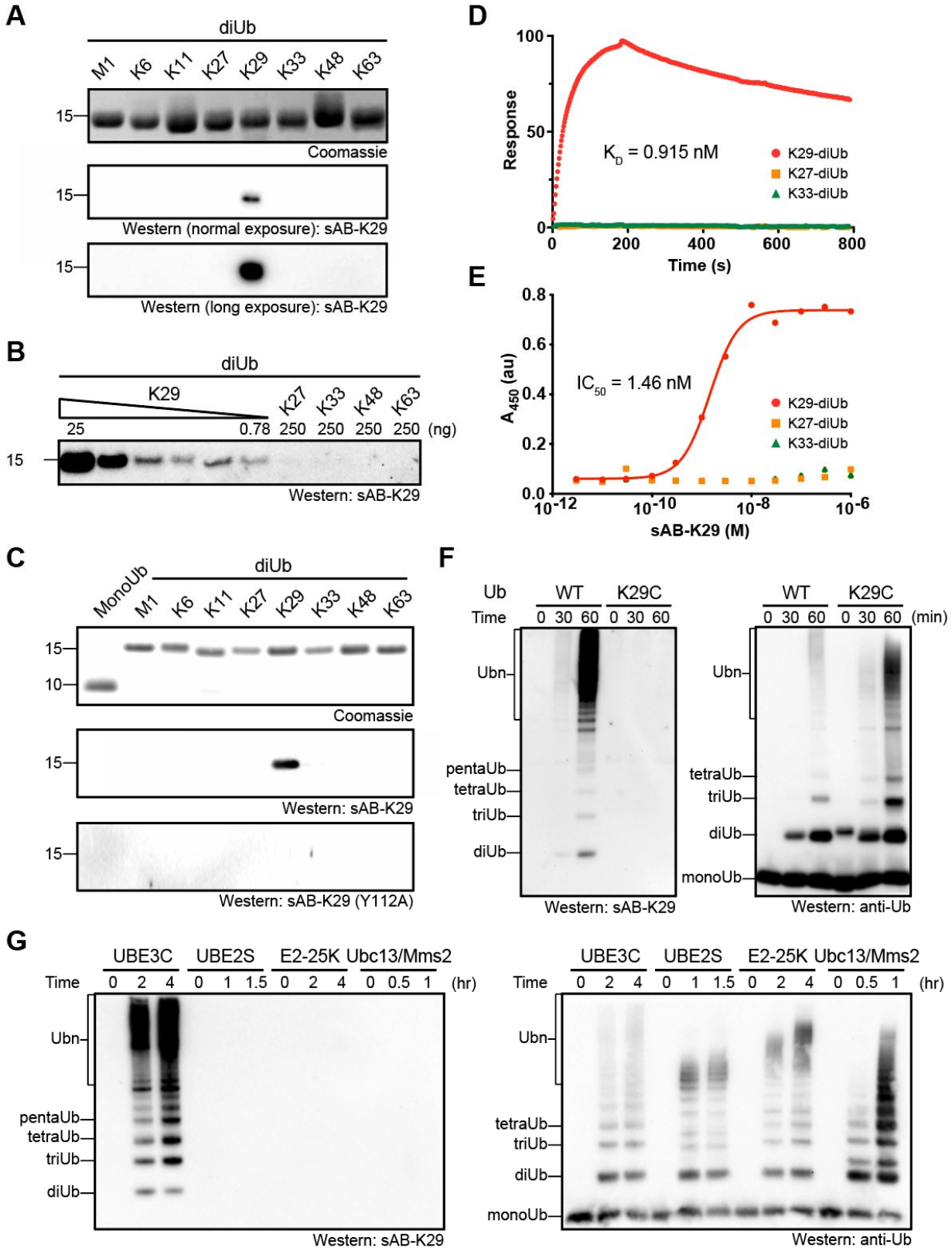

450

Figure 2. In vitro characterization of sAB-K29

(A) The specificity of sAB-K29. Diubiquitin molecules (~500 ng) with eight types of linkages were loaded on an SDS-PAGE gel. Western blotting was performed using sAB-K29 as the primary binder and peroxidase-conjugated goat anti-human IgG (F(ab)2 fragment-specific, Jackson ImmunoResearch) as the secondary antibody under normal or long exposure.

(B) The sensitivity and crossreactivity of sAB-K29. sAB-K29 could detect K29-linked diUb at the level of 0.78 ng in a Western blot and had no crossreactivity with K27/K33/K48/K63-linked diUb at the level of 250 ng.

(C) A point mutation in the heavy chain of sAB-K29 (Y112A) abolished its recognition of K29-linked diUb. Monoubiquitin and diubiquitin (~500 ng) with eight types of linkages were loaded on an SDS-PAGE gel. Western blotting was performed using sAB-K29 or sAB-K29 (Y112A) as the primary binder.

(D) Surface plasma resonance (SPR) experiments using immobilized K29/K27/K33-linked diUb and purified sAB-K29. The measured dissociation constant (K_D) of K29-linked diUb and sAB-K29 was 0.915 nM. No binding between sAB-K29 and K27/K33-linked diUb was detected.

(E) ELISAs using immobilized K29/K27/K33-linked diUb and a series of 12 serially diluted purified sAB-K29 solutions. The measured EC_{50} was 1.46 nM for K29-linked diUb. No significant absorption was detected for K27/K33-linked diUb.

(F) sAB-K29 could be used to detect K29-linked polyubiquitin chains assembled in vitro by Western blotting. K29-linked polyubiquitin chains were assembled by an E1-E2-E3 mixture containing UBE1, UBE2L3, and UBE3C. The reactions were followed for 60 minutes at three time points. Parallel Western blotting using anti-ubiquitin antibody was performed for comparison. The ubiquitin mutant K29C was used in the control experiment.

(G) sAB-K29 could specifically detect K29-linked polyubiquitin chains in vitro. Polyubiquitin chains were assembled by four ubiquitination systems: UBE3C (K48- and K29-linked chains),

UBE2S (K11-linked chains), E2-25K (K48-linked chains), and UBC13/Mms2 (K63-linked chains). Parallel Western blotting using anti-ubiquitin antibody was performed for comparison.

478 **FIGURE 3**

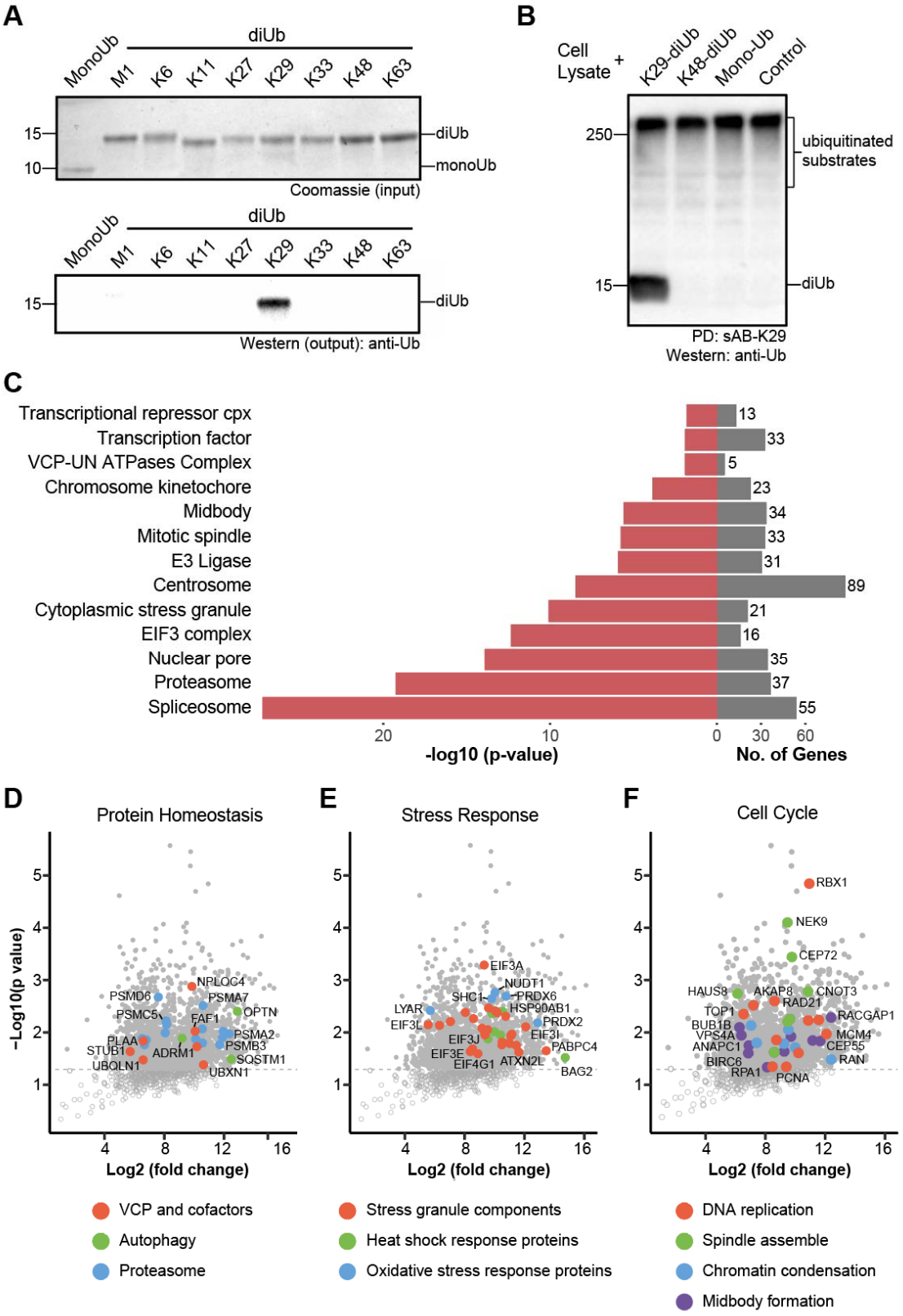

479

Figure 3. Pull-down and proteomic analyses of HeLa cells using sAB-K29

(A) sAB-K29 could be used to specifically pull down K29-linked diUb in vitro. Biotinylated sAB-K29 was used to pull down mono- and diubiquitin with eight types of linkages. Anti-ubiquitin antibody was used in Western blotting of the output.

(B) sAB-K29 could be used to specifically pull down K29-linked diUb and K29-linked polyubiquitin chains from cell lysates. Lysates of HeLa cells were mixed with K29- and K48-linked polyubiquitin and monoubiquitin. Biotinylated sAB-K29 was used for the pull-down experiment. Anti-ubiquitin antibody was used for Western blotting of the output.

(C) GO analysis (cellular components) of enriched proteins from pull-down experiments of HeLa cells using sAB-K29. The enriched proteins were identified using label-free quantitative mass spectrometry. Three biological and two technical replicates were performed. Significant hits (compared to pull-down using unconjugated beads, $p < 0.01$) were subjected to GO analysis.

(D-F) Volcano plots of the quantitative mass spectrometry results. Significant hits ($p < 0.05$) are colored blue, with those involved in protein homeostasis (D), the stress response (E), and the cell cycle (F) highlighted in red. Some well-documented proteins involved in each respective cellular process are labeled.

FIGURE 4

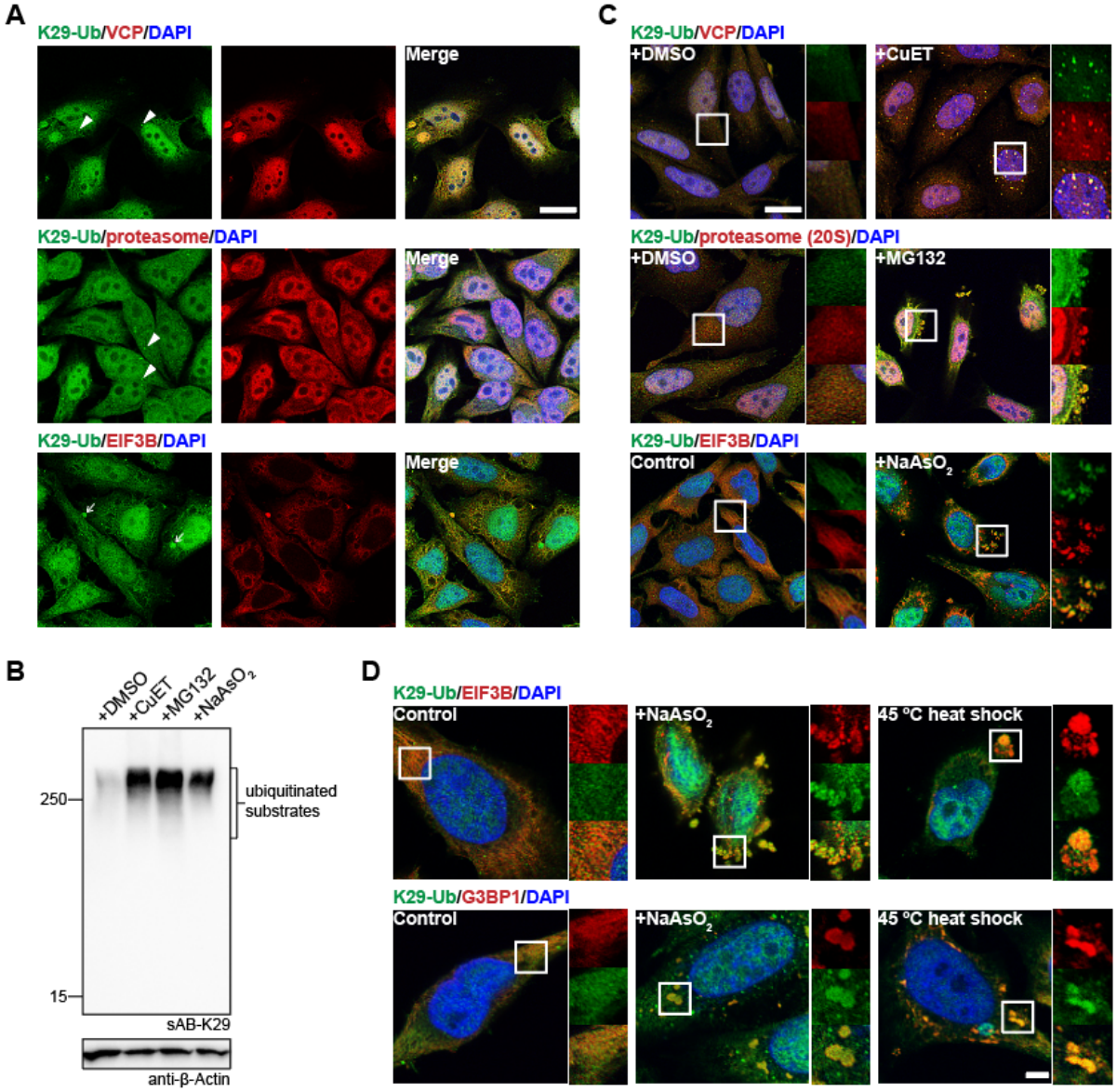

Figure 4. K29-linked polyubiquitination is involved in protein homeostasis and the stress response

(A) sAB-K29 was used for the immunofluorescent staining of untreated HeLa cells. Costaining for K29-Ub with VCP, the proteasome (20S), and EIF3B is shown. Arrowheads point to bright puncta stained by sAB-K29. Arrows point to liquid droplets stained by sAB-K29.

(B) K29-linked polyubiquitination was enhanced after HeLa cells were treated with CuET (an inhibitor of the VCP cofactor Npl4), MG132 (a proteasome inhibitor), or sodium arsenite (a stress response inducer). HeLa cells were treated with 1 μM CuET for 4 h, 100 μM MG132 for 4 h, or 500 μM NaAsO2 for 1 h, followed by Western blot analysis using sAB-K29 as the primary binder.

(C) Immunofluorescent staining of HeLa cells treated with 1 μM CuET for 4 h, 100 μM MG132 for 4 h, or 500 μM sodium arsenite for 1 h. Costaining for K29-Ub with VCP, the proteasome (20S), and EIF3B is shown.

(D) K29-linked polyubiquitination was enriched in stress granules. HeLa cells were treated with 500 μM sodium arsenite for 1 h or heat shocked at 45 °C for 30 minutes, followed by immunofluorescent staining. Costaining for K29-Ub with EIF3B and G3BP1 is shown.

Scale bars in panels A and C: 20 μm, panel D: 5 μm.

FIGURE 5

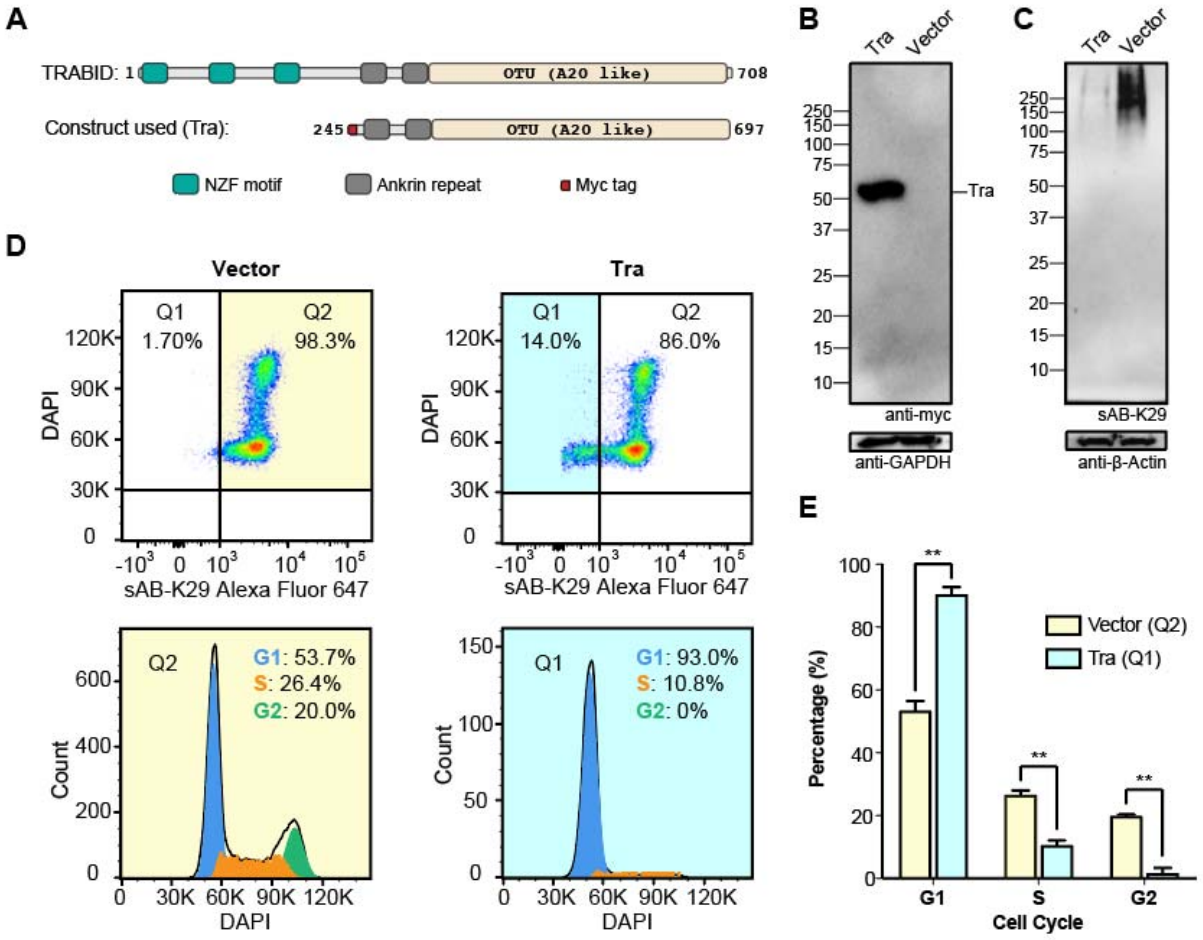

Figure 5. K29-linked polyubiquitination is involved in cell cycle regulation

(A) A truncated form of the human deubiquitinating enzyme (DUB) TRABID (residues 245-697, named Tra) was used to reduce the level of K29-linked polyubiquitination in HeLa cells. Domain diagrams of full-length TRABID and the Tra construct are shown.

(B and C) The expression and effect of Tra. HeLa cells were transfected with Tra or an empty vector for 27 h. The cell lysates were analyzed by Western blotting using c-myc antibody (B) and sAB-K29 (C), respectively.

(D) Cell cycle analysis of HeLa cells transfected with Tra or an empty vector for 27 h using flow cytometry. Representative flow cytometry graphs from two biological replicates are shown (a total of 5 injections). Highlighted areas were subjected to cell cycle analysis.

(E) Quantification of the cell cycle analysis results in panel D. Two biological replicates (a total of 5 injections) were included in this experiment. (**, $p < 0.01$ by two-tailed Student's *t*-test). Error bars represent standard deviations.

537 **FIGURE 6**

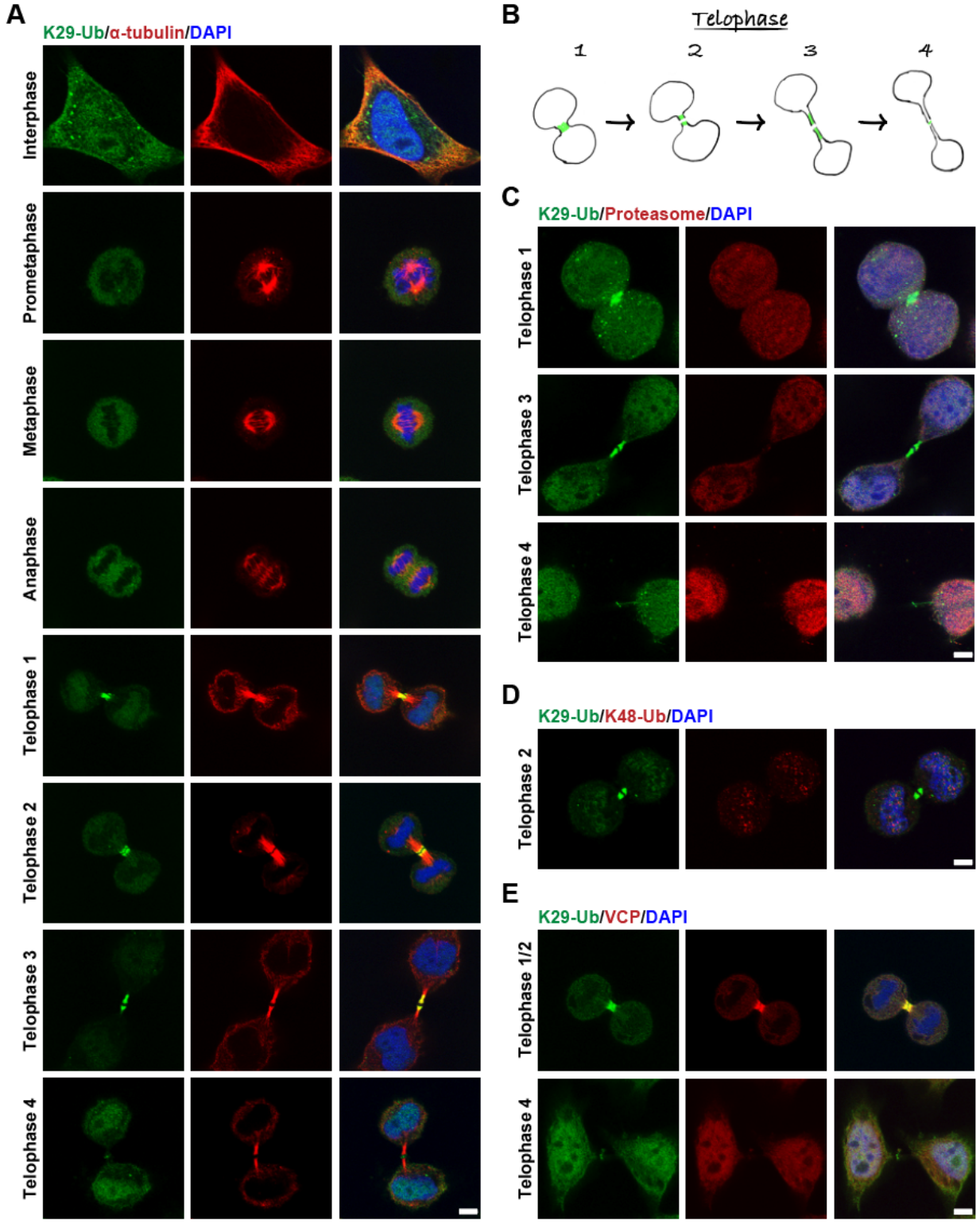

538

539

Figure 6. K29-linked polyubiquitination is enriched around the midbody during mitosis

(A) Immunofluorescent staining of HeLa cells in different stages of the cell cycle. Costaining for K29-Ub and β-tubulin is shown.

(B) A diagram showing migration of the K29-linked polyubiquitination signal during the telophase of mitosis. Roughly four stages could be distinguished based on localization and morphology.

(C) Immunofluorescent staining of HeLa cells at the telophase of mitosis. Costaining for K29-Ub and the proteasome (20S) is shown.

(D) Immunofluorescent staining of HeLa cells at the telophase of mitosis. Costaining for K29-Ub and K48-Ub (Abcam, cat# ab140601) is shown.

(E) Immunofluorescent staining of HeLa cells at the telophase of mitosis. Costaining for K29-Ub and VCP is shown.

Scale bars in panels A, C, D, and E correspond to 5 μm.

554 **FIGURE 7**

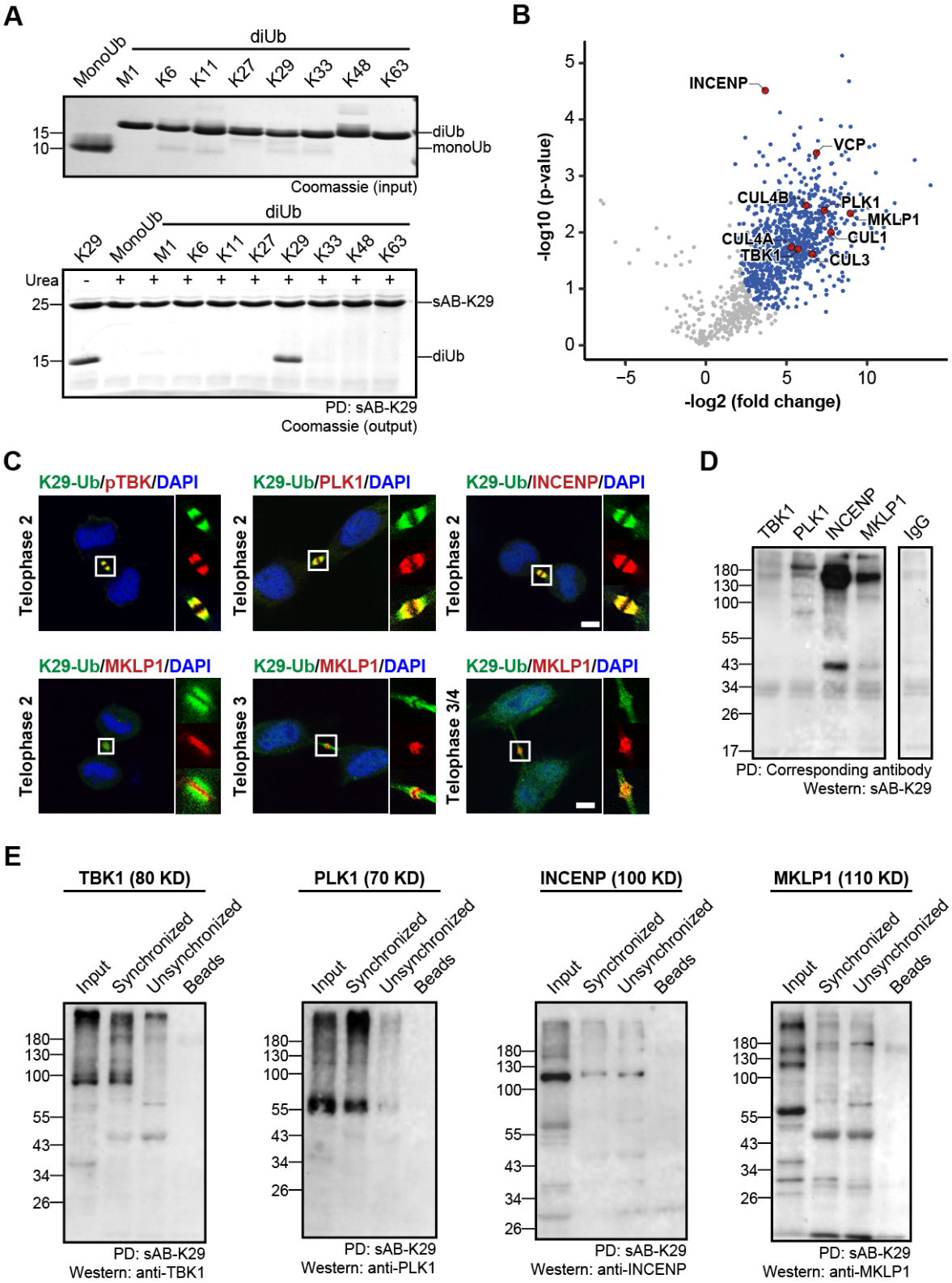

555

Figure 7. Midbody proteins involved in K29-linked polyubiquitination

(A) sAB-K29 could be used to specifically pull down K29-linked diUb under denaturing conditions (2 M urea).

(B) Volcano plot of the quantitative mass spectrometry results after pull-down experiments in HeLa cells synchronized to the telophase of mitosis using sAB-K29 under denaturing conditions (1 M urea). Significant hits (FDR < 0.05) are colored blue, with those involved in midbody assembly highlighted in red.

(C) Immunofluorescent staining of HeLa cells at the telophase of mitosis. Costaining for K29-Ub with pTBK, PLK1, INCENP, and MKLP1 is shown. Scale bars correspond to 5 μm.

(D) Immunoprecipitation of synchronized HeLa cells under denaturing conditions using antibodies against TBK1, PLK1, INCENP, and MKLP1. Western blotting was performed using sAB-K29 as the primary binder. Anti-IgG was used in the control experiment.

(E) Immunoprecipitation of HeLa cells (either synchronized to the telophase of mitosis or unsynchronized) using sAB-K29. Antibodies against TBK1, PLK1, INCENP, and MKLP1 were used for Western blotting.

CONTACT FOR REAGENT AND RESOURCES SHARING

Further information and requests for reagents and resources should be directed to the Lead Contact.

EXPERIMENTAL MODEL AND SUBJECT DETAILS

Mammalian cell culture

HeLa cells, 293T cells and A549 cells were cultured in Dulbecco's Modified Eagle's Medium (DMEM) supplemented with 10% Fetal Bovine Serum (FBS). Cells were tested for mycoplasma contamination. Plasmids were transfected using lipofectamine 3000 (Invitrogen).

METHOD DETAILS

Generation of K29-linked di-ubiquitin

K29-linked di-ubiquitin was generated as reported before (Kristariyanto et al., 2015b). Briefly, 2 mM wildtype ubiquitin was mixed with 1 μM UBA1, 10 μM Ubch7, and 10 μM UBE3C in a buffer containing 50 mM Tris (pH 7.5), 150 mM NaCl, 10 mM ATP, 10 mM $MgCl_2$, and 1 mM Tris(2-carboxyethyl)phosphine (TCEP), at 30 °C overnight. The reaction mixture were then incubated with 2 mM vOTU and 5 mM DTT at 30 °C overnight to remove non K29-linked ubiquitin chains. K29-linked di-ubiquitin was purified by cation exchange using a Mono S column (GE Healthcare) equilibrated in 50 mM NaOAc, pH 4.5. The column was eluted with a linear gradient of NaCl up to 1M. The peak corresponding to di-ubiquitin was pooled and further purified by gel filtration using a Superdex 75 column (GE Healthcare) equilibrated in 25 mM Tris, pH 8.0, 150 mM NaCl and 0.5 mM TCEP.

Generation of polyubiquitin chains

Polyubiquitin chains were generated as reported before (Michel et al., 2015). Briefly, wildtype ubiquitin or K29C mutant was mixed with UBA1 and specific combinations of E2 and E3 enzymes in a buffer containing 20 mMTris, pH 7.5, 150 mM NaCl, 10 mM ATP, 10 mM $MgCl_2$, and 1 mM TCEP. Specifically Ubch7/UBE3C were used to generate a mixture of polyubiquitin containing K29-linked chains; Ube2s, Ube25K, and Ubc13/Mms2 were used to generate K11-, K48- and K63-linked polyubiquitin chains, respectively. The reactions were monitored by Western Blot.

Purification of synthetic antibody fragment (sAB)

Plasmids containing sAB-K29 or sAB-MBP were transformed to E. coli BL21(DE3) cells for over-expression. Cells were collected and lysed in the Lysis Buffer (20 mM Tris-HCl, pH 7.4, 500 mM NaCl, 1 mM phenylmethylsulfonyl fluoride (PMSF)). The cell lysate was cleared by

centrifugation and run through a protein G-sepharose column equilibrated in the lysis buffer. The sABs were eluted using the Elution Buffer (0.1 M glycine, pH 2.7) and then cation-exchanged using a Mono S column equilibrated in Buffer A (50 mM sodium acetate pH 5.0). The proteins were eluted using a linear gradient of the sodium ions by mixing with Buffer B (50 mM sodium acetate pH 5.0, 2M NaCl).

Purification of other proteins

Plasmids containing UBA1 (homo sapiens), UBCH7 (homo sapiens), vOTU (the viral ovarian tumor DUB encoded by Crimean Congo hemorrhagic fever virus) were transformed to E. coli BL21(DE3) cells. UBA1 was over-expressed by IPTG induction, UBCH7 and vOTU were over-expressed by autoinduction following the established protocol (Studier, 2005). UBE3C was transformed to E. coli Rosseta 2 (DE3) cells and over-expressed by IPTG induction. The purification procedures followed the established protocols (Kristariyanto et al., 2015a; Michel et al., 2015). Briefly, *E. coli* cell pellets were resuspended in Lysis Buffer containing 50 mM Tris, pH 8.0, 300 mM KCl, 20 mM imidazole and 1 mM DTT with 1mM PMSF added freshly. Subsequently, cells were lysed by sonication, and the lysates were cleared by centrifugation at 16500 rpm for 30 min. Then the supernatants were flowed through a Ni–NTA gravity column twice at 4 °C. Beads were washed with Wash Buffer containing 50 mM Tris, pH 8, 150 mM NaCl and 25 mM imidazole. Finally, the His-tagged proteins were eluted in Elution Buffer containing 50 mM Tris, pH 8.0, 300 mM NaCl, 400 mM imidazole and 1mM DTT. For His-SUMO-Ube3c, SUMO protease (Ulp1p) were added to the eluate, and dialyzed in the buffer containing 25 mM Tris, pH 8.0, 150 mM NaCl and 0.5 mM TCEP. The proteins were further purified by a Superdex 200 gel filtration column (GE Healthcare) equilibrated in the buffer containing 25 mM Tris, pH 8.0, 150 mM NaCl and 0.5 mM TCEP.

Crystallization of sAB-K29 and K29-linked di-ubiquitin complex

Complex of sAB-K29 and K29-linked di-ubiquitin was formed by mixing purified sAB-K29 and K29-linked di-ubiquitin (1:1.5), followed by size exclusion chromatography using a Superdex 75 column equilibrated in a buffer containing 20 mM Tris-HCl, pH 7.4, 150 mM NaCl. Crystals were grown using the hanging drop method and appeared in 1 weeks at 21 °C from a 1:1 mixture of protein (18 mg/mL) and reservoir solution (0.1 M phosphate-citriate, 40% v/v Polyethylene glycol 300). Crystals were harvested and flash-frozen in liquid nitrogen without any cryo-protectant.

Data collection and structure determination

X-ray diffraction data were collected at the Northeastern Collaborative Access Team beamline (24-ID-E) at the Advanced Photon Source (Supplemental Table 1). The diffraction data were integrated and scaled using XDS/XSCALE (Kabsch, 2010). The structure was determined by molecular replacement using PHASER (Sliwiak et al., 2014) in PHENIX (Adams et al., 2010) and a Fab search model. The model was built using COOT (Emsley and Cowtan, 2004) and was refined using PHENIX. Coordinates and structure factor amplitudes have been deposited in the Protein Data Bank under accession number 7KEO.

Western blot

Western blots were performed using the standard protocol. Peroxidase-conjugated goat anti-human IgG, F(ab)2 fragment specific (Jackson ImmunoResearch, 109-036-006) was used as the secondary antibody (1:5000) when using sAB-K29 as the primary binder (0.2-2 μg/mL). Other primary antibodies are diluted as followed: Anti K63-Ub (Sigma,1:1000); Anti Ub (Abcam, 1:1000); Anti β-Actin (Santa Cruz, 1:1000), Anti GAPDH (Santa Cruz, 1:2000), Anti c-Myc (Genscript, 0.3 μg/mL), Anti VCP (Santa Cruz, 1:1000), Anti INCENP (Abcam,1:3000), Anti MKLP1 (Abcam,1:1000), Anti TBK1 (CST,1:1000), Anti PLK1 (Abcam, 1 μg/mL).

Phage Display

Four rounds of biopanning using Fab Library E (kind gift of A. Koide) were performed as follows using a protocol adapted from previous studies (Miller et al., 2012; Paduch et al., 2013). The first round of selection was performed manually using 300 nM of biotinylated K29-linked di-ubiquitin immobilized onto 250 µL of Streptavidin Paramagnetic Particles (Promega). Following washing with Selection Buffer (SB; 20 mM Hepes, pH 7.5, 150 mM NaCl, 0.5% BSA, 0.05% Tween-20), the beads were incubated with Library E for one hour at room temperature (RT). The beads were then washed three times with SB and used to directly infect log-phase *E. coli* XL-1 blue cells. Following infection, 2XYT media supplemented with ampicillin and M13 helper phage was added and phage were amplified overnight. To increase the stringency of selection, three additional rounds of sorting were performed in the presence of 1.5-µM of mono-ubiquitin as a competitor in solution. Further, the concentration of K29-linked di-ubiquitin was reduced each round as follows: 150 nM in round 2, 75 nM in round 3, and 15 nM in round 4. These three rounds were performed at RT semi-automatically using a Kingfisher magnetic beads handler. The overnight-amplified elution pool from each preceding round of selection was used as the input for the following round of sorting.

Single-point competitive phage ELISA

Elution pools from rounds 3 and 4 were used to infect log-phase *E. coli* XL-1 blue cells and plated onto LB-agar supplemented with ampicillin. Twenty-four colonies from each pool were picked and sequenced at the University of Chicago Comprehensive Cancer Center DNA Sequencing facility. DNA sequencing determined that 47 out of 48 colonies corresponded to a single clone, and both clones were tested for binding to K29-linked di-ubiquitin by ELISA. All ELISA were performed in 96-well plates (Nunc) coated with 2 µg/mL Neutravidin and blocked with phosphate-buffered saline containing 1% BSA. The plates were washed with ELISA Buffer (EB; 25 mM Hepes, pH 7.4, 150 mM NaCl, 0.05% Tween-20) and 25 nM of K29-linked Di-Ub (in

EB) was immobilized onto the plates. Amplified phage for both clones were diluted 20X into EB either in the absence or presence of competitors: non-biotinylated K29-linked di-ubiquitin, mono-ubiquitin, K27-linked di-ubiquitin, and K33-linked di-ubiquitin. Phage dilutions with and without competitors were added to target-immobilized ELISA plates, allowed to bind for 15 minutes, washed, and then incubated with an anti-M13 HRP-conjugated secondary antibody (GE Healthcare) for 30 minutes. Following washing with EB, bound phage were detected using TMB substrate kit (Thermo). Specificity was determined by comparing the ELISA signal with and without competition. Each assay was performed in triplicate.

Based on ELISA signal, only the most abundant clone from sequencing was found to be specific to K29-linked di-ubiquitin. This Fab, named sAB-K29, was then subcloned into the expression vector RH2.2 (kind gift of S. Sidhu) using the In-Fusion Cloning Kit (Takara) and sequence-verified.

Fab binding characterization

The binding of sAB-K29 to K29-linked di-ubiquitin was verified by multi-point ELISA (Dominik et al., 2016; Mukherjee et al., 2018) and surface plasmon resonance (SPR). ELISA were performed using plates prepared as above. Biotinylated constructs of K29-, K27-, and K33-linked di-ubiquitin were immobilized individually onto ELISA plates at 25 nM final concentrations. Twelve serial dilutions of sAB-K29, starting at 1 µM concentration, were prepared in EB and each Fab dilution was bound to wells containing either immobilized targets or no targets (to determine any background signal). Following washing with EB, bound Fab was detected by incubation with an anti-Fab HRP-conjugated secondary (Jackson) and TMB substrate kit, as above. The quenched absorbance signal was measured and plotted as a function of the log of Fab concentration. EC_{50} values were then calculated in GraphPad using a variable slope model and assuming sigmoidal dose response. Each assay was performed in triplicate and the mean signal was used to fit the dose response curve.

SPR experiments were performed using a MASS-1 instrument (Bruker) with a His-capture sensor chip (XanTec). His-tagged constructs of K29, K27, and K33-linked di-ubiquitin were immobilized onto sensor chips following coating of the experimental and reference channels with 0.5 mM $NiSO_4$. His-tagged proteins (ligands) were immobilized only in the experimental channels. After optimization of the amount of immobilized ligands based on response units (RUs), a series of sAB-K29 concentrations was injected into both the experimental and reference channels. sAB-K29 was injected over a 60s-association phase, followed by a 600s dissociation time (Mukherjee et al., 2018). Following each injection, the chip surface was regenerated using 350 mM EDTA and 50 mM NaOH, and ligands were subsequently immobilized for the following injection. For each ligand, all experiments were performed on single channels for consistency. Fab injections were then double-reference subtracted using the reference channel signal and a buffer-only experimental channel injection. The double-reference subtracted curves were then fit with one-to-one Langmuir binding models in Scrubber to determine kinetic binding parameters, which are given in the attached table.

Immunoprecipitation for mass spectrometry

Biotinylated sAB-K29 (100 µg) was incubated with 1 mL streptavidin-magnetic beads (Promega, Z5482) prewashed three times with PBS buffer in a thermo shaker for 3 h at 25 °C. The beads containing immobilized sAB-K29 were then incubated with 5 mg of HeLa cell lysate in RIPA lysis buffer (P0013B, Beyotime) on a rotation wheel at 4 °C overnight. The beads were washed 3 times with the wash buffer containing 25 mM Tris-HCl, pH 8.0, 500 mM NaCl, and 0.5 % Triton, followed by 3 times with the wash buffer without Triton. The bound proteins were eluted with 100 µl 8M Urea for 1h at 25 °C in a thermo shaker. Similar procedures were followed for immunoprecipitation under the denaturing condition (denature IP), except that 5 mg of synchronized HeLa cell lysate in 8 M Urea with protease inhibitor cocktail (Roche, 4693116001) was diluted by PBS buffer to a final urea concentration of 1 M before incubating with the

conjugated beads. Each experiment was performed in triplicate and eluted fractions were pooled and analyzed by SDS-PAGE or Western blot.

Sample preparation for tandem mass tag (TMT) mass spectrometry

Proteins extracted by immunoprecipitation were subjected to disulfide bond reduction with 25 mM DTT in 50 mM NH_4HCO_3 for 60 min at 55 °C followed by alkylation in 55 mM iodoacetamide in 50 mM NH_4HCO_3 for 60 min at 37 °C. Samples were digested overnight at 37 °C with trypsin (1:50, w/w) (Promega, V5280), followed by acidification with 1% formic acid for 15 min and subjected to C18 solid-phase extraction using Sep-Pak (Waters). Tandem mass tag labeling of each sample (20ug) was performed by adding 20 ng/mL stock of TMT reagent along with acetonitrile to achieve a final acetonitrile concentration of approximately 30% (v/v). Following incubation at room temperature for 1 h, the reaction was quenched with hydroxylamine to a final concentration of 0.5% (v/v) for 15 min. The TMT-labeled samples were pooled together at a 1:1 ratio. The sample was vacuum centrifuged to near dryness, and subjected to C18 solid-phase extraction using Sep-Pak (Waters). Dried TMT-labeled sample was resuspended in 100 mL of 10mM NH_4HCO_3, pH 8.0 and fractionated using basic pH reversed-phase (BPRP) HPLC. Briefly, samples were offline fractionated over a 90 min run, into 96 fractions by BPRP HPLC through an aeris peptide xb-c18 column (Phenomenex; 250 mm x 3.6 mm) with mobile phase A containing 5% acetonitrile and 10 mM NH_4HCO_3 in LC-MS grade H_2O, and mobile phase B containing 90% acetonitrile and 10 mM NH4HCO3 in LC-MS grade H_2O (both pH 8.0). The 96 resulting fractions were then pooled into 12 fractions which were used for subsequent mass spectrometry analysis. Fractions were vacuum centrifuged to near dryness.

Sample preparation for label free mass spectrometry

Eluted protein fractions by denature IP were incubated in 20 µl 4 × LDS loading buffer (NP0007, Thermo Fisher) for 5 min at 95 °C. Proteins were separated on 4%-12% gradient gels

(NP0336Box, Thermo Fisher) and stained with Coomassie blue G-250 (161-0436, Bio-Rad). For in-gel digestion, each gel lane was cut into 6 bands which were then cut into smaller (around 1 mm) fragments. Gel pieces were de-stained in 50 mM NH_4HCO_3/ACN (1:1, v/v). After washing with 50 mM NH_4HCO_3, proteins were reduced by the addition of 25 mM DTT in 50 mM NH_4HCO_3 for 60 min at 55 °C followed by alkylation in 55 mM iodoacetamide in 50 mM NH_4HCO_3 for 60 min at 37 °C. After washing in 50 mM NH_4HCO_3/ACN (1:1, v/v) and dehydration in ACN, proteins were digested overnight at 37 °C with trypsin (1:50, w/w) (V5280, Promega). Peptides were extracted from the gel in 50% ACN/0.1% formic acid, followed by vacuum drying and re-dissolved by 20 µl 0.1 % formic acid for LC-MS analysis.

Mass spectrometry data collection

Tryptic peptides were separated on an UltiMate 3000 RSLCnano System (Thermo Scientific, USA) at a flow rate of 300 nL/min using a 120 min gradient from 5% ACN, 0.1% formic acid to 45% ACN, 0.1% formic acid followed by a washing step at 100% ACN. Each of the 3 independent biological replicates was measured as technical duplicates. Mass spectra were collected on a Thermo Orbitrap Fusion Lumos mass spectrometer (Thermo Fisher Scientific). For TMT-labeling, each analysis used the Multi-Notch MS3-based TMT method to reduce ion interference as compared to MS2 quantification. For label free, each analysis was operated in data dependent top-speed mode with dynamic exclusion set at 30 s and a total cycle time of 3 s. Full scan MS spectra were acquired in the Orbitrap at a resolution of 120000 (at m/z 200) with an automatic gain control ion target value of 4e5 and a maximum injection time of 50 ms. The most intense precursors with charge states of 2-7 and intensities greater than 5e3 were selected for MS/MS experiments using higher-energy collisional dissociation (HCD) with 27 % collision energy. Isolation was performed in the quadrupole with an automatic gain control ion target value of 2e3 and a maximum injection time of 300 ms.

Mass spectrometry data analysis and quantification

Raw data from LC-MS/MS measurements were analyzed using MaxQuant version 1.6.5.0 with default settings and either TMT-labeling or label-free quantification (LFQ) enabled. For protein identification, the human reference proteome downloaded from the UniProt database (download date: 2019-07-01) and an integrated database of common contaminants was used. Identified proteins were filtered for reverse hits and common contaminants at a false discovery rate of 1%. Further data processing was performed using Perseus software (version 1.5.8.5) and R software (version 3.6.1).

Immunofluorescence staining and imaging

HeLa cells were fixed with 4% paraformaldehyde in PBS at room temperature for 20 min, washed three times with PBS. Nonspecific binding sites were blocked with 10% normal goat serum, 0.1% Triton X-100 for 1 h at room temperature. The cells were then stained for 2 h at room temperature with the primary binder / antibody. After that, the cells were washed three times with PBS containing 0.1% TritonX-100, following by staining for 1 h with the secondary antibody. Finally, cells were washed three times with PBS containing 0.1% Triton X-100, and mounted with ProLong Gold Antifade reagent with DAPI (Invitrogen). Alexa Fluor 488 or 647 conjugated $F(ab')_2$ fragment goat anti-human IgG, F(ab')2 fragment specific (Jackson ImmunoResearch) was used as the secondary antibody (1:500) when using sAB-K29 as the primary binder (2 μg/mL). Other primary antibodies are diluted as followed: Anti AuroraB (Fisher,1:500); Anti □-Tubulin (Genscript, 1:50-1:100); Anti □-Tubulin (proteintech, 1:200); Anti c-Myc (Genscript, 0.5 μg/mL); Anti EIF3B (Santa Cruz, 1:100); Anti INCENP (Santa Cruz,1:100), Anti MKLP1(Santa Cruz, 1:100); Anti Proteasome 20S core subunits (Fisher, 1:250); Anti K48-Ub (Abcam, 1:200); Anti VCP (Santa Cruz,1:200); Anti G3BP1 (proteintech,1:500); Anti pTBK1 (cell signaling,1:50); Anti PLK1 (Santa Cruz,1:50). Images were collected by a Leica SP5 2-photon laser scanning confocal microscope.

Super-resolution microscopy

sAB-K29 was labeled with Alexa Fluor 647 (A647, Invitrogen A20006) following the instructions of Alexa Fluor Protein Labeling Kits (Thermo Fisher). Unreacted free dye was removed using P-6 Gel Columns (Bio-Rad). The labeling efficiency is about 1 Alexa Fluor 647 dye per antibody. 3D STORM imaging was conducted as previously described (Fei et al., 2015) on an inverted microscope using a 647 nm laser and a 405 nm laser and data were recorded by an EMCCD camera. For 3D imaging, a cylindrical lens was placed in the emission beam path. Each STORM image was reconstructed from about 5,000 image frames. Imaging buffer was composed of 10 mM NaCl, 50 mM Tris (pH 8), 10% glucose, 50 U/mL glucose oxidase (Sigma Aldrich G2133-10KU), 404 U/mL catalase (EMD Millipore 219001) and 20mM cysteamine (Sigma Aldrich 30070-10G). 3D Image reconstruction and visualization was conducted as previously described (Park et al., 2018).

Cellular stress assays

HeLa cells were treated with CuET (1 μM, 4h, this paper), MG132(100μM, 4h, Sigma-Aldrich) $NaAsO_2$ (500 μM, 1h, Sigma), Cycloheximide (100 μg/ml, 6h, Sigma), Puromycine (1 μg/ml,2h, GoldBio), α-Amanitin (5 μg/ml, 24h, MCE), or 45 °C heat shock for 30 min. K29-ubquitin chains was detected by western blot or immunofluorescence microscopy.

Cell synchronization

HeLa cells were first synchronized in G1/S-phase with 2 mM thymidine for 24h, followed by PBS wash and releasing to fresh DMEM/10% FBS media for 3h. After that, cells were treated with 50 ng/ml nocodazole for 12h and arrested in prometaphase. For progression through mitosis, cells were harvested via pipetting, washed with PBS twice, and released into fresh media. Cell lysates were taken at indicated time points and analyzed via western blot.

Flow cytometry

Cells were transfected with the Tra construct (human TRABID, 245-697) or the pCMV vector using lipofectamine 3000 for 27 h before harvesting and washing with PBS. The cells were fixed with either 1% or 4% PFA for 15 min at room temperature, followed by washing with PBS and permeabilization with 70% ethanol at 4 °C overnight. Nonspecific binding was blocked with 2% BSA. The cells were then incubated with Anti-c-myc antibody conjugated with PE (sc-40, Santa Cruz Biotechnology) and sAB-K29 labeled with Alexa Fluor 647 for 1h at room temperature, followed by washing with PBS. Finally, the cells were incubated with Hoechst dye at room temperature for 15 min, followed by washing with PBS. The data was acquired by a LSRFortessa X-20 cell analyzer (BD) and analysis by flowjo.

SUPPLEMENTAL TABLES

TABLE S1. X-ray data collection and refinement statistics

Data collection	
Space group	C2
Cell dimensions	
a, *b*, *c* (Å)	186.6, 43.74, 174.8
α, β, γ (°)	90, 107.8, 90
Resolution (Å)	2.9 (2.98-2.90) *
R_{sym} or R_{merge}	0.162 (0.977)
$CC_{1/2}$ (%)	99.1 (57.0)
$I / \sigma I$	6.72 (1.46)
Completeness (%)	98.1 (98.2)
Redundancy	3.7 (3.7)
Refinement	
Resolution (Å)	19.7 – 2.9
No. reflections	30022
R_{work} / R_{free}	23.6 / 28.2
No. atoms	
Protein	8846
Ligand/ion	30
Water	13
B-factors	
Protein	62.4
Ligand/ion	71.8
Water	48.4
R.m.s. deviations	
Bond lengths (Å)	0.002
Bond angles (°)	0.461

*Values in parentheses are for highest-resolution shell.

SUPPLEMENTAL FIGURE LEGENDS

FIGURE S1

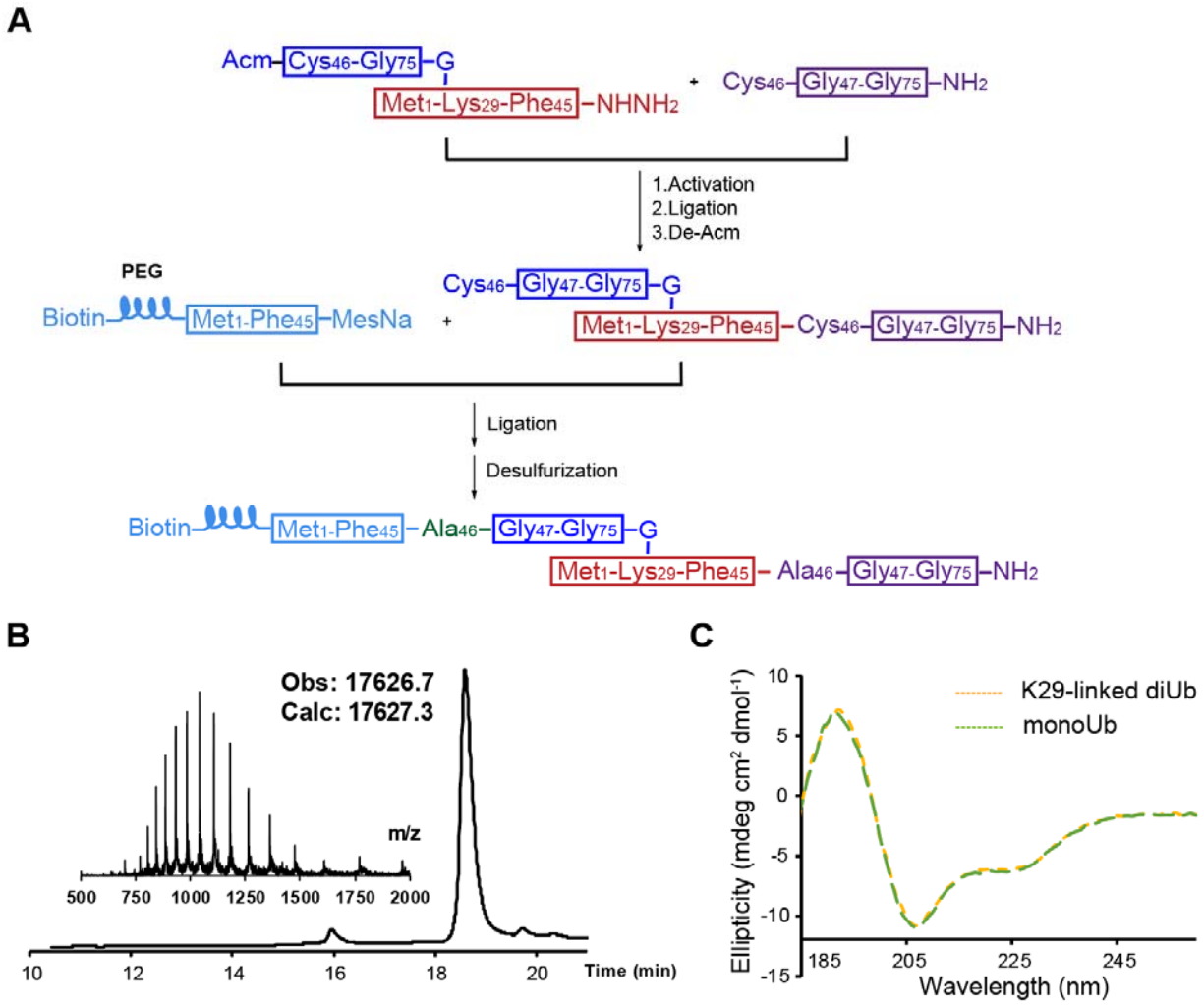

Figure S1. Chemical synthesis and characterization of biotinylated K29-linked diubiquitin

(A) Synthetic routes for biotinylated K29-linked diubiquitin.

(B) Liquid chromatography and mass spectrometry (LC-MS) analysis of synthetic biotinylated K29-linked diubiquitin.

(C) Circular dichroism (CD) spectra of synthetic biotinylated K29-linked diubiquitin and recombinant monoubiquitin.

FIGURE S2

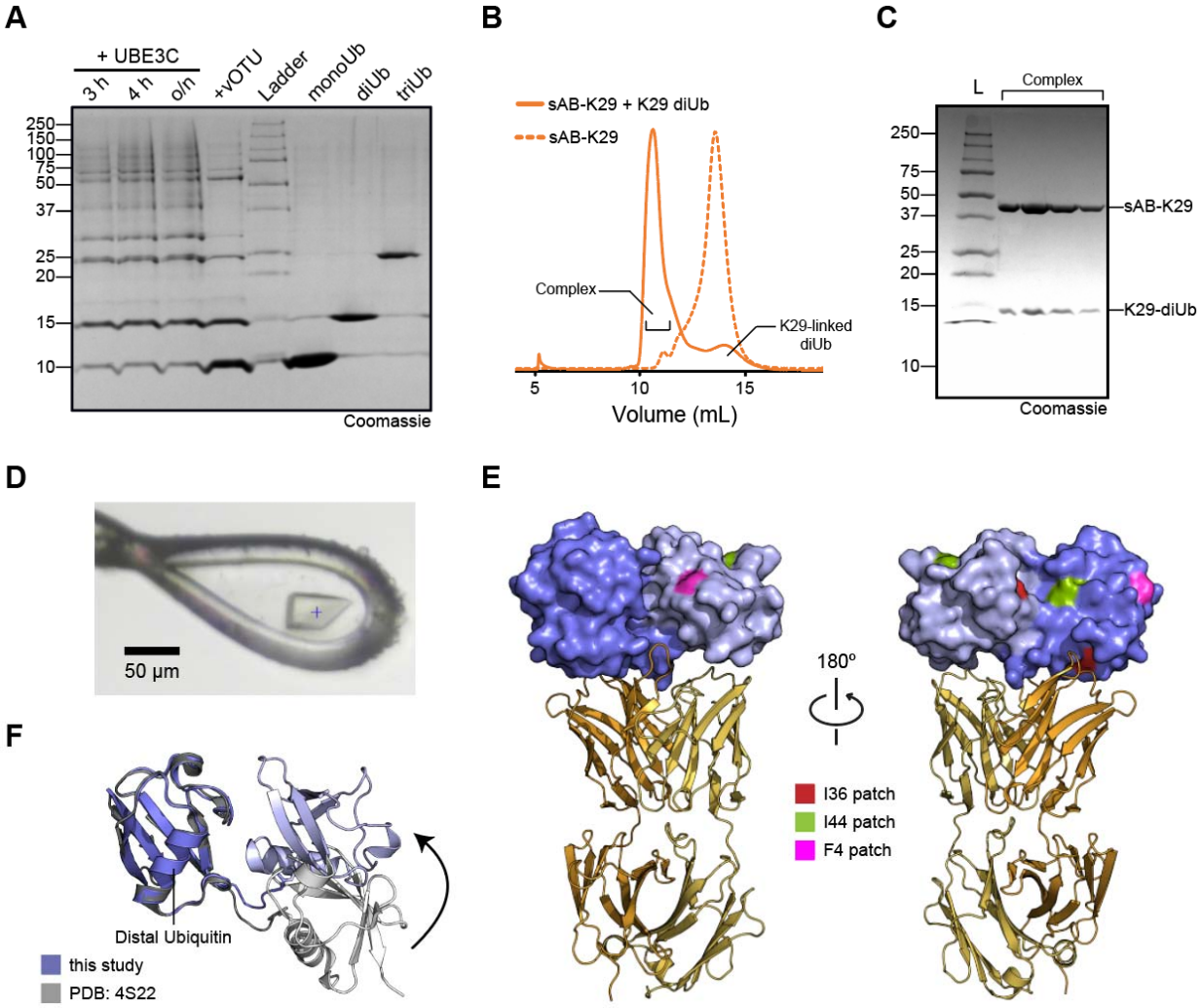

Figure S2. Purification and crystallization of the complex between K29-linked diubiquitin and sAB-K29

(A) Purification of K29-linked diubiquitin. A mixture of K29- and K48-linked polyubiquitin mixture was assembled by incubating monoubiquitin, UBE1, UBE2L3, and UBE3C overnight. vOTU, a DUB that does not cleave K29-linked chains, was added to the reaction mixture to cleave K48-linked polyubiquitin chains. The resulting mono-, di-, and triubiquitin molecules were separated by anion exchange chromatography.

(B) Size exclusion chromatography (SEC) of sAB-K29 and sAB-K29 in complex with K29-linked diubiquitin.

(C) The SDS-PAGE gel of the complex peak in panel B.

(D) A picture of the crystal of the complex mounted in a cryo-loop. Diffraction data were collected at APS beamline NECAT.

(E) The distribution of hydrophobic patches on K29-linked diUb. Only the I36 patch of the distal ubiquitin molecule is involved in the interaction with the heavy chain of sAB-K29.

(F) Superposition of the crystal structure of K29-linked diUb (PDB accession code: 4S22) and K29-linked diUb in the complex structure determined in this study. The distal ubiquitin molecules in the two structures were aligned.

FIGURE S3

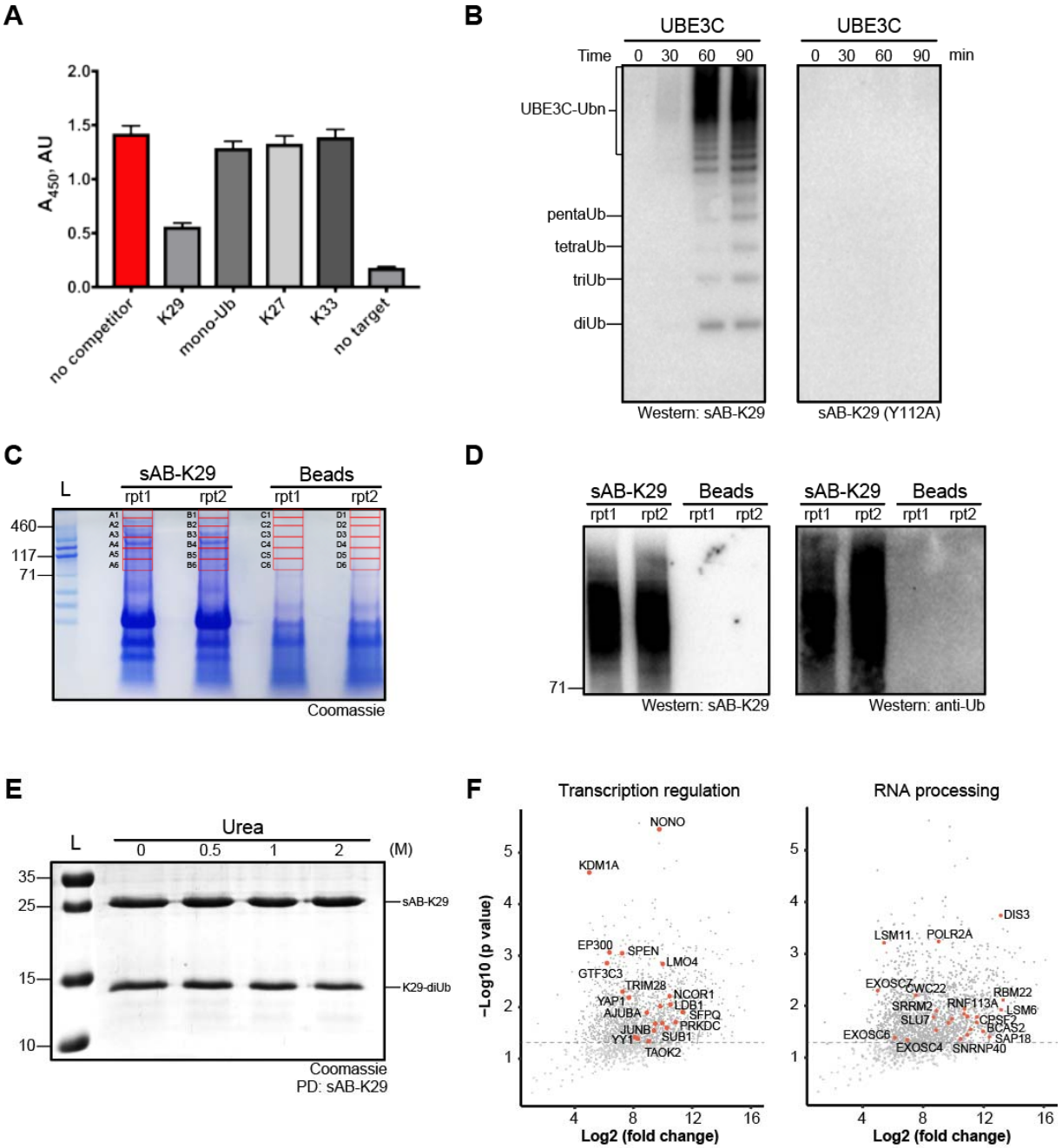

Figure S3. Characterization of sAB-K29 specificity and pull-down experiments

(A) Single-point competitive phage ELISA. Biotinylated K29-linked diubiquitin was immobilized and incubated with phage-displayed sAB-K29 in the presence of excess competitors (monoubiquitin and K29-, K27-, and K33-linked diubiquitin) in solution. A decrease in absorption

indicated more specific binding. Error bars represent the standard deviations of triplicate experiments.

(B) Mutation of the heavy chain of sAB-K29 (Y112A) abolished its ability to detect K29-linked polyubiquitin chains by Western blotting. K29-linked polyubiquitin chains were assembled by an E1-E2-E3 mixture containing UBE1, UBE2L3, and UBE3C. The reactions were followed for 90 minutes at four time points.

(C) Pull-down assay of HeLa cell lysate using sAB-K29. The bound proteins were separated on an SDS-PAGE gel. Gel slices in red frames were subjected to label-free quantitative mass spectrometry to identify the enriched proteins. Two biological replicates were performed. Unconjugated beads were used in the control pull-down assay.

(D) Western blot analysis of the pull-down eluate in panel C. sAB-K29 or anti-ubiquitin antibody was used as the primary binder.

(E) sAB-K29 could be used to pull down K29-linked diUb in vitro under denaturing conditions (up to 2 M urea).

(F) Volcano plots of the quantitative mass spectrometry results. Significant hits ($p < 0.05$) are above the dotted line, with those involved in transcription regulation and RNA processing highlighted. Some well-documented proteins are labeled.

FIGURE S4

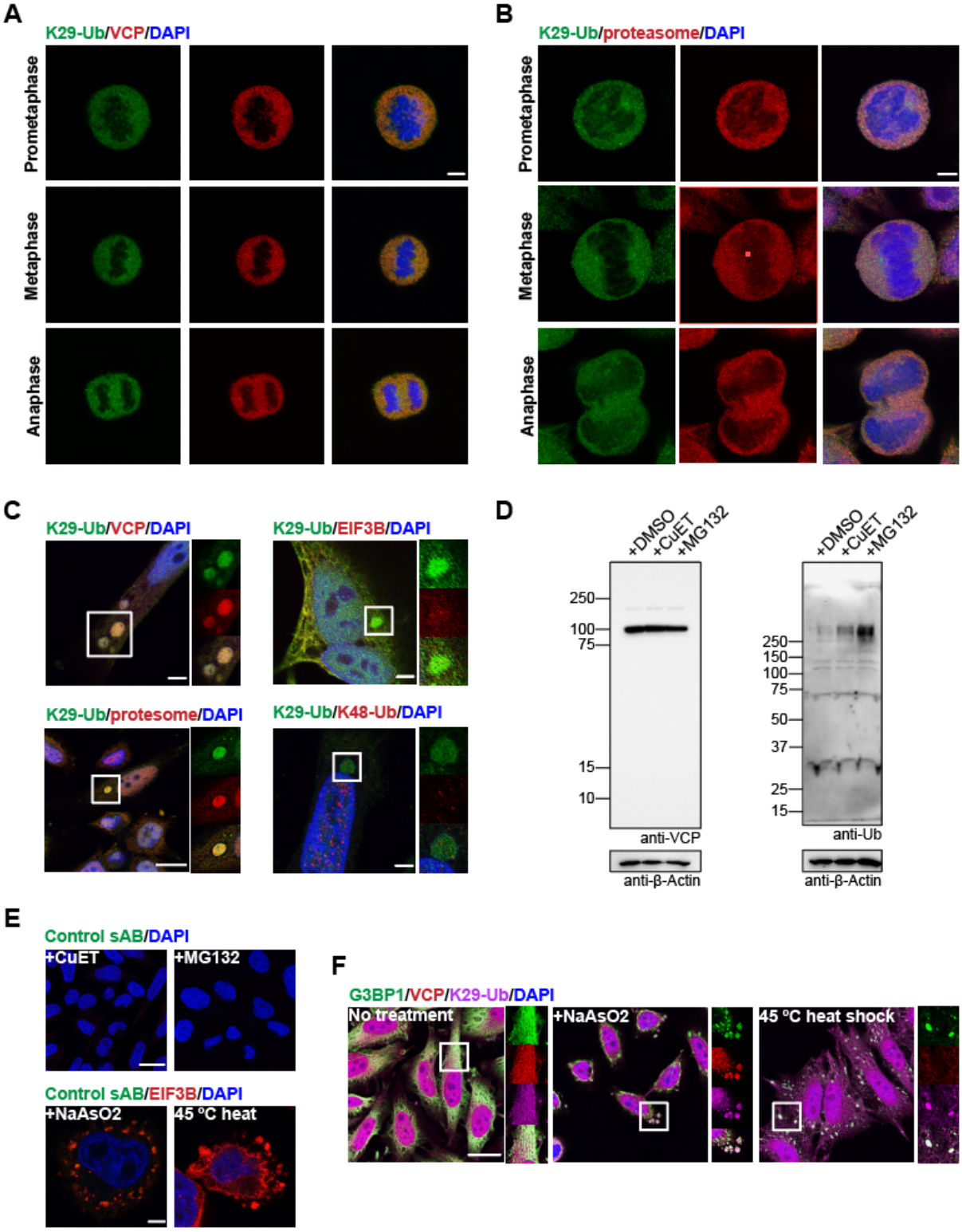
A
K29-Ub/VCP/DAPI
Prometaphase
Metaphase
Anaphase
B
K29-Ub/proteasome/DAPI
Prometaphase
Metaphase
Anaphase
C
K29-Ub/VCP/DAPI
K29-Ub/EIF3B/DAPI
K29-Ub/protesome/DAPI
K29-Ub/K48-Ub/DAPI
D
+DMSO
+CuET
+MG132
250
100
75
15
10
anti-VCP
anti-β-Actin
+DMSO
+CuET
+MG132
250
150
100
75
50
37
25
15
anti-Ub
anti-β-Actin
E
Control sAB/DAPI
+CuET
+MG132
Control sAB/EIF3B/DAPI
+NaAsO2
45 °C heat
F
G3BP1/VCP/K29-Ub/DAPI
No treatment
+NaAsO2
45 °C heat shock

Figure S4. K29-linked ubiquitination is involved in protein homeostasis and the stress response

(A and B) Immunofluorescent staining of HeLa cells at prometaphase, metaphase, and anaphase of mitosis. Costaining for K29-Ub with VCP (panel A) or the proteasome (20S, panel B) is shown. Scale bars correspond to 5 μm.

(C) K29-linked ubiquitination is enriched in liquid droplets occasionally observed in normal HeLa cells. Costaining for K29-Ub with VCP, EIF3B, the proteasome (20S), and K48-Ub is shown.

(D) Western blots of VCP and total ubiquitin in HeLa cells treated with CuET (inhibitor of the VCP cofactor Npl4, 1 μM for 4 h) or MG132 (a proteasome inhibitor, 100 μM MG132 for 4 h). The scale bar in the bottom left panel corresponds to 5 μm. Other scale bars correspond to 20 μm.

(E) Immunofluorescent staining of HeLa cells with a control sAB (against maltose-binding protein) and costaining for EIF3B in HeLa cells treated with 500 μM sodium arsenite for 1 h or subjected to heat shock at 45 °C for 30 minutes. Scale bars in the top and bottom panels correspond to 20 and 5 μm, respectively.

(F) Immunofluorescent staining of HeLa cells treated with 500 μM sodium arsenite for 1 h or subjected to heat shock at 45 °C for 30 minutes. Costaining for K29-Ub with G3BP1 and VCP is shown. The scale bar corresponds to 20 μm.

FIGURE S5

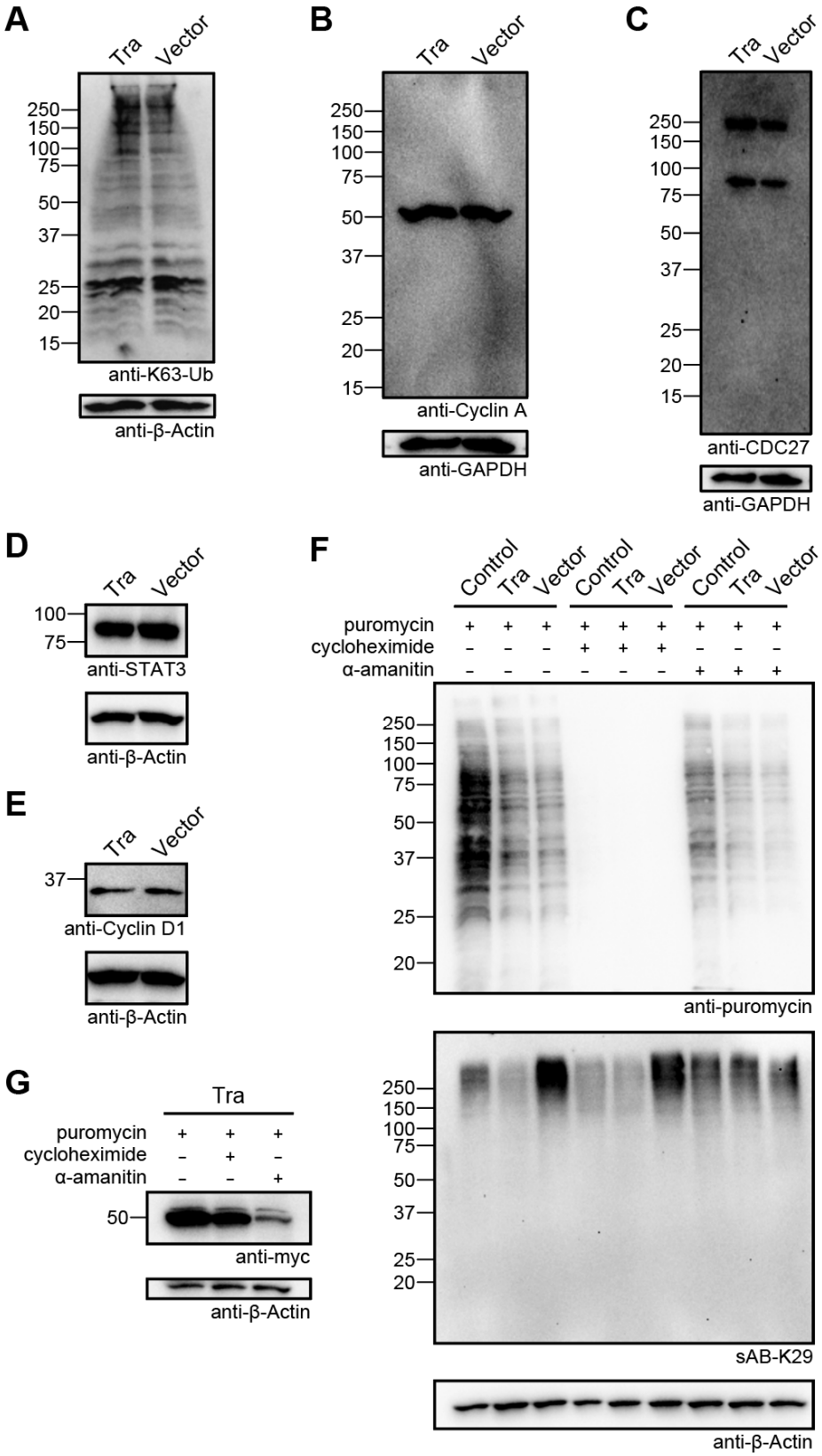
A
Tra
Vector
250
150
100
75
50
37
25
20
15
anti-K63-Ub
anti-β-Actin
B
Tra
Vector
250
150
100
75
50
37
25
20
15
anti-Cyclin A
anti-GAPDH
C
Tra
Vector
250
150
100
75
50
37
25
20
15
anti-CDC27
anti-GAPDH
D
Tra
Vector
100
75
anti-STAT3
anti-β-Actin
E
Tra
Vector
37
anti-Cyclin D1
anti-β-Actin
F
Control
Tra
Vector
Control
Tra
Vector
Control
Tra
Vector
puromycin + + + + + + + + +
cycloheximide – – – + + + – – –
α-amanitin – – – – – – + + +
250
150
100
75
50
37
25
20
anti-puromycin
250
150
100
75
50
37
25
20
sAB-K29
anti-β-Actin
G
Tra
puromycin + + +
cycloheximide – + –
α-amanitin – – +
50
anti-myc
anti-β-Actin

Figure S5. Western blot analysis of HeLa cells after the level of K29-linked ubiquitination was reduced using the Tra construct

(A-E) Western blots of K63-linked ubiquitin, CyclinA, CDC 27, STAT3, and Cyclin D1 in HeLa cells transfected with the Tra construct or control vector.

(F) New protein synthesis was not affected after K29-linked ubiquitination was reduced in HeLa cells. HeLa cells were transfected with the Tra construct or control vector and treated with puromycin, cycloheximide, or α-amanitin. Western blotting was performed using anti-puromycin antibody or sAB-K29.

(G) Expression level of the Tra construct in HeLa cells treated with puromycin, cycloheximide, or α-amanitin. Western blotting was performed using an anti-cMyc antibody.

FIGURE S6

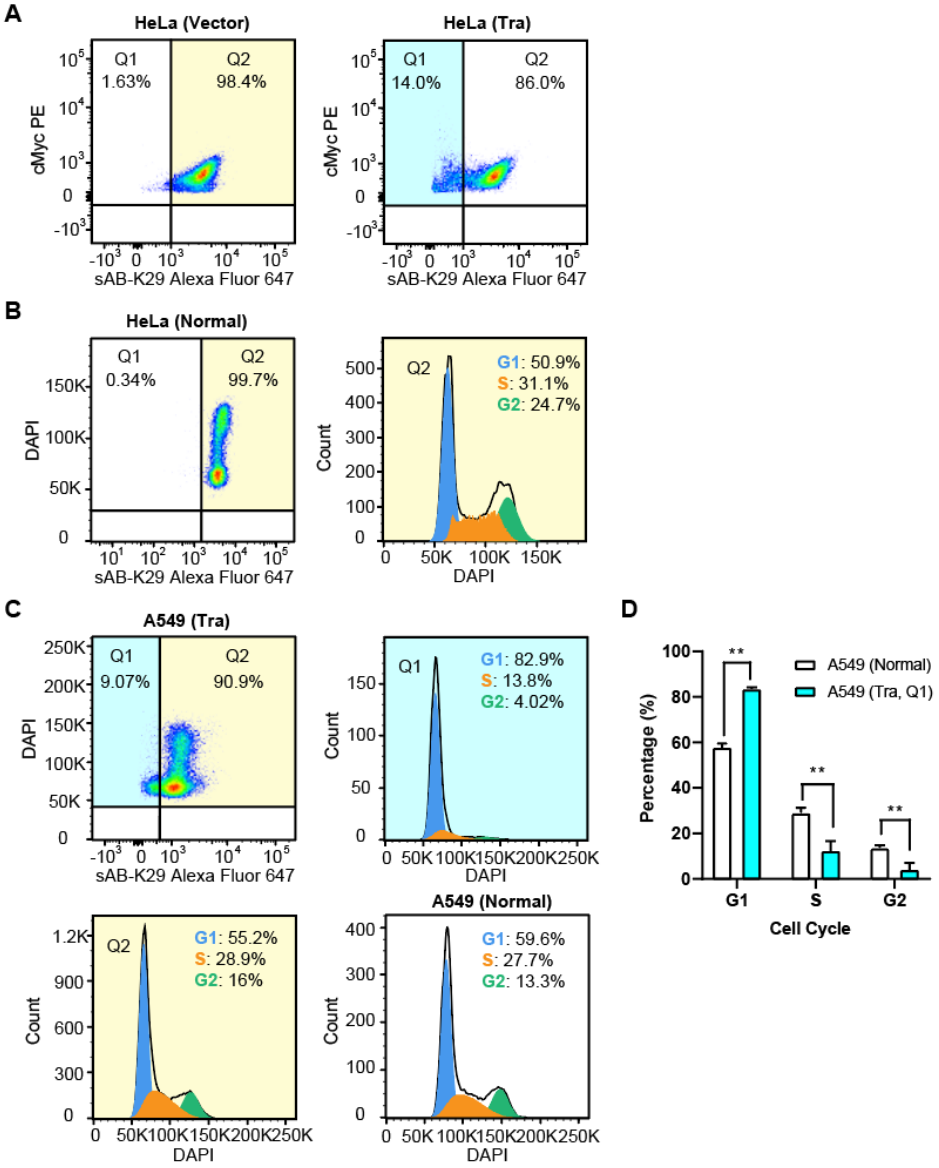

Figure S6. Reduced K29-linked ubiquitination led to G1 arrest

(A) Cell cycle analysis of HeLa cells transfected with either the Tra construct or empty vector by flow cytometry. cMyc and K29-linked polyubiquitin channels are shown. Note that the cMyc tag was also expressed in cells transfected with the empty vector. Representative flow cytometry graphs from two biological replicates are shown.

(B) Cell cycle analysis of normal HeLa cells by flow cytometry.

(C) Cell cycle analysis of A549 cells transfected with either the Tra construct or empty vector by flow cytometry.

(D) Quantification of the A549 cell cycle analysis results in panel C. Error bars represent standard deviations from three injections (**, $p < 0.01$ by two-tailed Student's *t*-test).

968 **FIGURE S7**

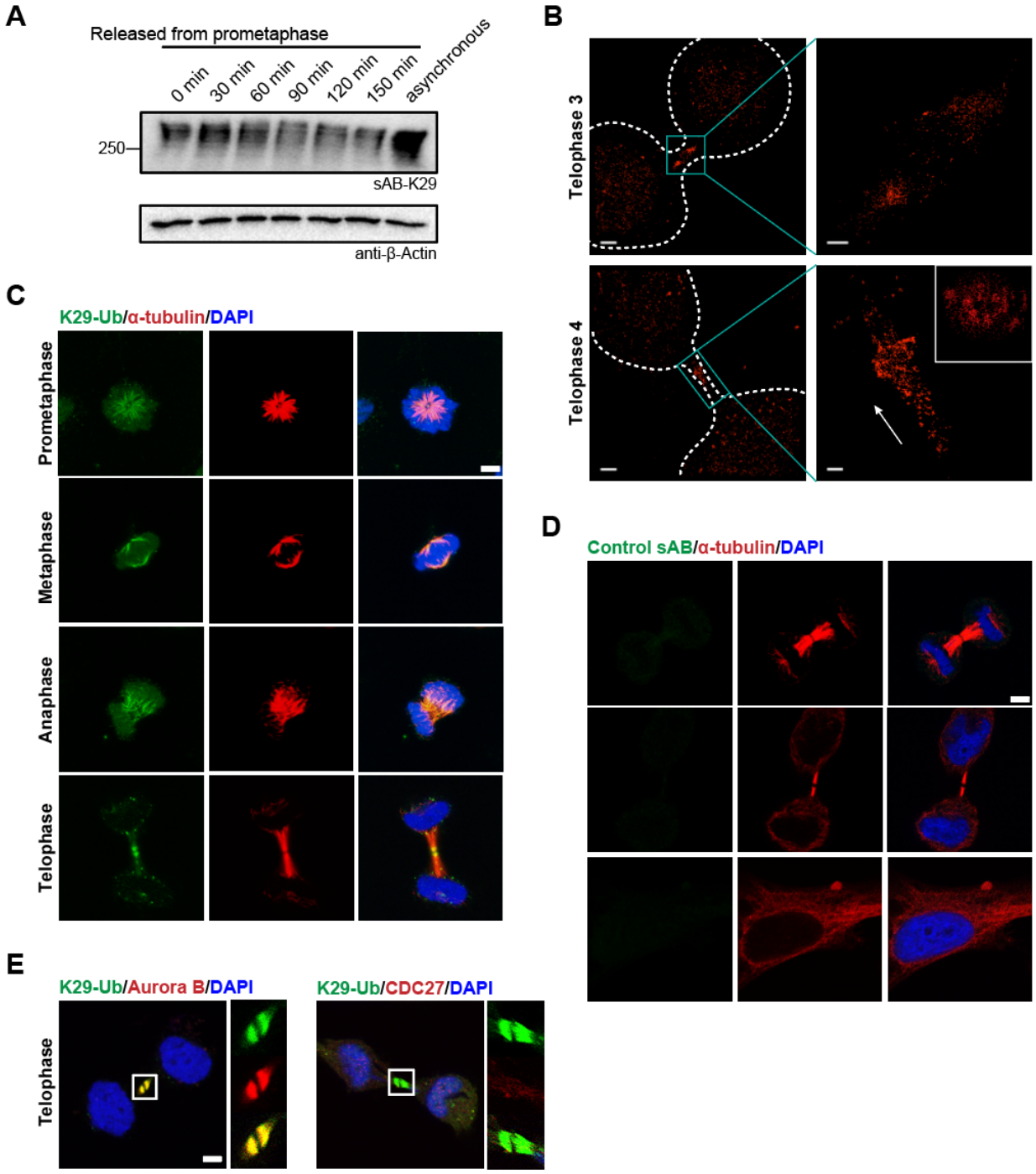

969

970 **Figure S7. K29-linked ubiquitination is involved in mitosis**

971 (A) Western blot analysis of K29-linked ubiquitination during mitosis. HeLa cells were

972 synchronized to prometaphase by treatment with thymidine and nocodazole. Aliquots of cells

were taken and lysed at the indicated time points, followed by Western blotting using sAB-K29 as the primary binder.

(B) 3D STORM images of K29-linked polyubiquitin at telophase 3 and 4. The orthographic projection image of the highlighted area in telophase 4 (bottom cyan box) along the long axis (white arrow) is shown in the upper right inset. Rendering was conducted by Visual Molecular Dynamics (VMD) with GLSL rendering, Orthographic display, and Surf drawing. Movies showing rotation are presented as Movies S1A and S1B. Scale bars in the left images correspond to 2 μm. Scale bars in the right images correspond to 500 nm.

(C) Immunofluorescent staining of HeLa cells at different stages of mitosis. Costaining for K29-linked ubiquitin with α-tubulin is shown. Cells were pre-extracted before fixation.

(D) Immunofluorescent staining of HeLa cells with a control sAB (against maltose-binding protein). Costaining for α-tubulin is shown. Cells were pre-extracted before fixation.

(E) Immunofluorescent staining of HeLa cells at the telophase of mitosis. Costaining for K29-linked ubiquitin with either Aurora B or CDC27 (a negative control) is shown. Cells were pre-extracted before fixation.

Scale bars in panels C, D, and E correspond to 5 μm.

Movie S1

3D STORM visualization of K29-linked ubiquitin. Rendering was conducted by Visual Molecular Dynamics (VMD) with GLSL rendering, Orthographic display, and Surf drawing.

(A) Rotation by a shorter axis.

(B) Rotation by a longer axis.

REFERENCES

Adams, P.D., Afonine, P.V., Bunkóczi, G., Chen, V.B., Davis, I.W., Echols, N., Headd, J.J., Hung, L.-W., Kapral, G.J., Grosse-Kunstleve, R.W.*, et al.* (2010). PHENIX: a comprehensive Python-based system for macromolecular structure solution. Acta crystallographica Section D, Biological crystallography *66*, 213-221.

Antos, J.M., Truttmann, M.C., and Ploegh, H.L. (2016). Recent advances in sortase-catalyzed ligation methodology. Curr Opin Struct Biol *38*, 111-118.

de la Pena, A.H., Goodall, E.A., Gates, S.N., Lander, G.C., and Martin, A. (2018). Substrate-engaged 26S proteasome structures reveal mechanisms for ATP-hydrolysis-driven translocation. Science *362*.

Dikic, I., Wakatsuki, S., and Walters, K.J. (2009). Ubiquitin-binding domains - from structures to functions. Nat Rev Mol Cell Biol *10*, 659-671.

Ding, Z., Xu, C., Sahu, I., Wang, Y., Fu, Z., Huang, M., Wong, C.C.L., Glickman, M.H., and Cong, Y. (2019). Structural Snapshots of 26S Proteasome Reveal Tetraubiquitin-Induced Conformations. Mol Cell *73*, 1150-1161 e1156.

Dominik, P.K., Borowska, M.T., Dalmas, O., Kim, S.S., Perozo, E., Keenan, R.J., and Kossiakoff, A.A. (2016). Conformational Chaperones for Structural Studies of Membrane Proteins Using Antibody Phage Display with Nanodiscs. Structure *24*, 300-309.

Dong, Y., Zhang, S., Wu, Z., Li, X., Wang, W.L., Zhu, Y., Stoilova-McPhie, S., Lu, Y., Finley, D., and Mao, Y. (2019). Cryo-EM structures and dynamics of substrate-engaged human 26S proteasome. Nature *565*, 49-55.

Emsley, P., and Cowtan, K. (2004). Coot: Model-building tools for molecular graphics. Acta Crystallographica Section D: Biological Crystallography *60*, 2126-2132.

Fei, J., Singh, D., Zhang, Q., Park, S., Balasubramanian, D., Golding, I., Vanderpool, C.K., and Ha, T. (2015). RNA biochemistry. Determination of in vivo target search kinetics of regulatory noncoding RNA. Science *347*, 1371-1374.

Haakonsen, D.L., and Rape, M. (2019). Branching Out: Improved Signaling by Heterotypic Ubiquitin Chains. Trends Cell Biol *29*, 704-716.

Hicke, L., Schubert, H.L., and Hill, C.P. (2005). Ubiquitin-binding domains. Nat Rev Mol Cell Biol *6*, 610-621.

Ikeda, F., and Dikic, I. (2008). Atypical ubiquitin chains: new molecular signals. 'Protein Modifications: Beyond the Usual Suspects' review series. EMBO Rep *9*, 536-542.

Jolly, C., Usson, Y., and Morimoto, R.I. (1999). Rapid and reversible relocalization of heat shock factor 1 within seconds to nuclear stress granules. P Natl Acad Sci USA *96*, 6769-6774.

Kabsch, W. (2010). XDS. Acta Crystallographica Section D: Biological Crystallography *66*, 125-132.

Karim, M., Biquand, E., Declercq, M., Jacob, Y., van der Werf, S., and Demeret, C. (2020). Nonproteolytic K29-Linked Ubiquitination of the PB2 Replication Protein of Influenza A Viruses by Proviral Cullin 4-Based E3 Ligases. mBio *11*.

Keusekotten, K., Elliott, P.R., Glockner, L., Fiil, B.K., Damgaard, R.B., Kulathu, Y., Wauer, T., Hospenthal, M.K., Gyrd-Hansen, M., Krappmann, D.*, et al.* (2013). OTULIN antagonizes LUBAC signaling by specifically hydrolyzing Met1-linked polyubiquitin. Cell *153*, 1312-1326.

Komander, D., and Rape, M. (2012). The ubiquitin code. Annu Rev Biochem *81*, 203-229.

Kristariyanto, Y.A., Abdul Rehman, S.A., Campbell, D.G., Morrice, N.A., Johnson, C., Toth, R., and Kulathu, Y. (2015a). K29-selective ubiquitin binding domain reveals structural basis of specificity and heterotypic nature of k29 polyubiquitin. Molecular cell *58*, 83-94.

Kristariyanto, Y.A., Abdul Rehman, S.A., Campbell, D.G., Morrice, N.A., Johnson, C., Toth, R., and Kulathu, Y. (2015b). K29-selective ubiquitin binding domain reveals structural basis of specificity and heterotypic nature of k29 polyubiquitin. Mol Cell *58*, 83-94.

Kulathu, Y., and Komander, D. (2012). Atypical ubiquitylation - the unexplored world of polyubiquitin beyond Lys48 and Lys63 linkages. Nat Rev Mol Cell Biol *13*, 508-523.

Li, Y.M., Li, Y.T., Pan, M., Kong, X.Q., Huang, Y.C., Hong, Z.Y., and Liu, L. (2014). Irreversible site-specific hydrazinolysis of proteins by use of sortase. Angew Chem Int Ed Engl *53*, 2198-2202.

Licchesi, J.D., Mieszczanek, J., Mevissen, T.E., Rutherford, T.J., Akutsu, M., Virdee, S., El Oualid, F., Chin, J.W., Ovaa, H., Bienz, M.*, et al.* (2011). An ankyrin-repeat ubiquitin-binding domain determines TRABID's specificity for atypical ubiquitin chains. Nat Struct Mol Biol *19*, 62-71.

Lopez-Mosqueda, J., and Dikic, I. (2014). Deciphering functions of branched ubiquitin chains. Cell *157*, 767-769.

Matsumoto, M.L., Dong, K.C., Yu, C., Phu, L., Gao, X., Hannoush, R.N., Hymowitz, S.G., Kirkpatrick, D.S., Dixit, V.M., and Kelley, R.F. (2012). Engineering and structural characterization of a linear polyubiquitin-specific antibody. J Mol Biol *418*, 134-144.

Matsumoto, M.L., Wickliffe, K.E., Dong, K.C., Yu, C., Bosanac, I., Bustos, D., Phu, L., Kirkpatrick, D.S., Hymowitz, S.G., Rape, M.*, et al.* (2010). K11-linked polyubiquitination in cell cycle control revealed by a K11 linkage-specific antibody. Mol Cell *39*, 477-484.

Mevissen, T.E.T., and Komander, D. (2017). Mechanisms of Deubiquitinase Specificity and Regulation. Annu Rev Biochem *86*, 159-192.

Meyer, H., Bug, M., and Bremer, S. (2012). Emerging functions of the VCP/p97 AAA-ATPase in the ubiquitin system. Nat Cell Biol *14*, 117-123.

Meyer, H.J., and Rape, M. (2014). Enhanced protein degradation by branched ubiquitin chains. Cell *157*, 910-921.

Michel, M.A., Elliott, P.R., Swatek, K.N., Simicek, M., Pruneda, J.N., Wagstaff, J.L., Freund, S.M., and Komander, D. (2015). Assembly and specific recognition of k29- and k33-linked polyubiquitin. Mol Cell *58*, 95-109.

Michel, M.A., Swatek, K.N., Hospenthal, M.K., and Komander, D. (2017). Ubiquitin Linkage-Specific Affimers Reveal Insights into K6-Linked Ubiquitin Signaling. Mol Cell *68*, 233-246 e235.

Miersch, S., Li, Z., Hanna, R., McLaughlin, M.E., Hornsby, M., Matsuguchi, T., Paduch, M., Saaf, A., Wells, J., Koide, S.*, et al.* (2015). Scalable high throughput selection from phage-displayed synthetic antibody libraries. J Vis Exp, 51492.

Miller, K.R., Koide, A., Leung, B., Fitzsimmons, J., Yoder, B., Yuan, H., Jay, M., Sidhu, S.S., Koide, S., and Collins, E.J. (2012). T cell receptor-like recognition of tumor in vivo by synthetic antibody fragment. PLoS One *7*, e43746.

Mukherjee, S., Griffin, D.H., Horn, J.R., Rizk, S.S., Nocula-Lugowska, M., Malmqvist, M., Kim, S.S., and Kossiakoff, A.A. (2018). Engineered synthetic antibodies as probes to quantify the energetic contributions of ligand binding to conformational changes in proteins. Journal of Biological Chemistry *293*, 2815-2828.

Newton, K., Matsumoto, M.L., Wertz, I.E., Kirkpatrick, D.S., Lill, J.R., Tan, J., Dugger, D., Gordon, N., Sidhu, S.S., Fellouse, F.A.*, et al.* (2008). Ubiquitin chain editing revealed by polyubiquitin linkage-specific antibodies. Cell *134*, 668-678.

Paduch, M., Koide, A., Uysal, S., Rizk, S.S., Koide, S., and Kossiakoff, A.A. (2013). Generating conformation-specific synthetic antibodies to trap proteins in selected functional states. Methods *60*, 3-14.

Pan, M., Gao, S., Zheng, Y., Tan, X., Lan, H., Tan, X., Sun, D., Lu, L., Wang, T., Zheng, Q.*, et al.* (2016). Quasi-Racemic X-ray Structures of K27-Linked Ubiquitin Chains Prepared by Total Chemical Synthesis. J Am Chem Soc *138*, 7429-7435.

Pan, M., Zheng, Q., Gao, S., Qu, Q., Yu, Y., Wu, M., Lan, H., Li, Y., Liu, S., Li, J.*, et al.* (2019). Chemical Synthesis of Structurally Defined Phosphorylated Ubiquitins Suggests Impaired Parkin Activation by Phosphorylated Ubiquitins with a Non-Phosphorylated Distal Unit. CCS Chemistry *1*, 476-489.

Pan, M., Zheng, Q., Yu, Y., Ai, H., Xie, Y., Zeng, X., Wang, C., Liu, L., and Zhao, M. (2020). Seesaw Conformations of Npl4 in the Human p97 Complex and the Inhibitory Mechanism of a Disulfiram Derivative. BioRxiv.

Park, S., Zhang, J., Reyer, M.A., Zareba, J., Troy, A.A., and Fei, J. (2018). Conducting Multiple Imaging Modes with One Fluorescence Microscope. J Vis Exp.

Ramadan, K., Bruderer, R., Spiga, F.M., Popp, O., Baur, T., Gotta, M., and Meyer, H.H. (2007). Cdc48/p97 promotes reformation of the nucleus by extracting the kinase Aurora B from chromatin. Nature *450*, 1258-1262.

Scheffner, M., Nuber, U., and Huibregtse, J.M. (1995). Protein ubiquitination involving an E1-E2-E3 enzyme ubiquitin thioester cascade. Nature *373*, 81-83.

Skrott, Z., Mistrik, M., Andersen, K.K., Friis, S., Majera, D., Gursky, J., Ozdian, T., Bartkova, J., Turi, Z., Moudry, P.*, et al.* (2017). Alcohol-abuse drug disulfiram targets cancer via p97 segregase adaptor NPL4. Nature *552*, 194-199.

Sliwiak, J., Jaskolski, M., Dauter, Z., McCoy, A.J., and Read, R.J. (2014). Likelihood-based molecular-replacement solution for a highly pathological crystal with tetartohedral twinning and sevenfold translational noncrystallographic symmetry. Acta crystallographica Section D, Biological crystallography *70*, 471-480.

Studier, F.W. (2005). Protein production by auto-induction in high density shaking cultures. Protein expression and purification *41*, 207-234.

Swatek, K.N., and Komander, D. (2016). Ubiquitin modifications. Cell Res *26*, 399-422.

Tsai, W.C., Gayatri, S., Reineke, L.C., Sbardella, G., Bedford, M.T., and Lloyd, R.E. (2016). Arginine Demethylation of G3BP1 Promotes Stress Granule Assembly. J Biol Chem *291*, 22671-22685.

Tsuchiya, H., Burana, D., Ohtake, F., Arai, N., Kaiho, A., Komada, M., Tanaka, K., and Saeki, Y. (2018). Ub-ProT reveals global length and composition of protein ubiquitylation in cells. Nature communications *9*, 524-524.

van Huizen, M., and Kikkert, M. (2019). The Role of Atypical Ubiquitin Chains in the Regulation of the Antiviral Innate Immune Response. Front Cell Dev Biol *7*, 392.

Wang, G., Gao, Y., Li, L., Jin, G., Cai, Z., Chao, J.I., and Lin, H.K. (2012). K63-linked ubiquitination in kinase activation and cancer. Front Oncol *2*, 5.

Yau, R., and Rape, M. (2016). The increasing complexity of the ubiquitin code. Nat Cell Biol *18*, 579-586.

Yau, R.G., Doerner, K., Castellanos, E.R., Haakonsen, D.L., Werner, A., Wang, N., Yang, X.W., Martinez-Martin, N., Matsumoto, M.L., Dixit, V.M.*, et al.* (2017). Assembly and Function of Heterotypic Ubiquitin Chains in Cell-Cycle and Protein Quality Control. Cell *171*, 918-933 e920.